Oxidation Chemistry of Metal-Bonded C_4 Chains: A Combined Chemical, Spectroelectrochemical, and Computational Study

Michael I. Bruce,*[,†,‡] Paul J. Low,[†,§] Karine Costuas,[||] Jean-François Halet,*[,||] Stephen P. Best,[⊥] and Graham A. Heath[#]

Contribution from the Department of Chemistry, University of Adelaide, Adelaide, South Australia 5005, Australia, Laboratoire de Chimie du Solide et Inorganique Moléculaire, UMR CNRS 6511, Université de Rennes 1, 35042 Rennes Cedex, France, School of Chemistry, The University of Melbourne, Parkville, Victoria 3052, Australia, and Research School of Chemistry, Australian National University, Canberra, ACT 0200, Australia

Received June 14, 1999

Abstract: The known complex $\{Cp(PPh_3)_2Ru\}_2(\mu\text{-}C{\equiv}CC{\equiv}C)$ (**3-Ph**) and its PMe_3-substitution product $\{Cp(PPh_3)(PMe_3)Ru\}_2(\mu\text{-}C{\equiv}CC{\equiv}C)$ (**3-Me**) have been shown by cyclic voltammetry to undergo a series of four stepwise one-electron oxidation processes. Successive oxidation potentials (V) for the first three reversible processes of **3-Ph** (**3-Me**) are −0.23 (−0.26), +0.41 (+0.33), and +1.03 (+0.97); the fourth, irreversible oxidation at +1.68 (+1.46) V is accompanied by chemical transformation followed by further oxidation. Chemical oxidation of **3-Ph** with 1 or 2.5 equiv of $AgPF_6$ in CH_2Cl_2/1,2-dimethoxyethane gave the one- and two-electron oxidized species [**3-Ph**][PF_6] and [**3-Ph**][PF_6]$_2$, respectively. The chemical and electrochemical studies have been complemented by a series of detailed spectroelectrochemical experiments to obtain spectral data associated with the $\mathbf{3}^{n+}$ ($n = 0-4$) species from 1500 to 40 000 cm^{-1}, without necessitating the isolation of each individual species. Theoretical techniques have been employed in order to probe the structure of the conjugated all-carbon ligand at each stage of oxidation. Both the metal centers and the carbon atoms of the C_4 bridge are affected, with removal of electrons housed in MOs delocalized over all atoms of the Ru−C_4−Ru chain. Comparison of models with different ligand surroundings suggests that molecules containing strong electron-donating ligands should be more easily oxidized.

Introduction

Complexes which display ligand-mediated electronic effects, including electron-transfer phenomena, have attracted a great deal of interest for many years.[1−3] Many of the pioneering efforts in this area played an important role in establishing various aspects of mechanistic chemistry[4,5] and in unraveling some of the key steps in complicated biological reactions, including respiration and photosynthesis. More recently, research in this area has focused on the potential applications of these compounds in the preparation of advanced materials which display unusual magnetic[6] or nonlinear optical properties.[7−9] Ligands capable of mediating electronic effects are also under investigation as potential molecular wires which are required for use in the assembly of nanoscale electronic devices.[10] Ligands based on linear polycarbon chains, C_n, have emerged as some of the most efficient "wires" examined to date.[11,12]

Polycarbon moieties based on yndiyl (−C≡C−) and polyyndiyl (−{C≡C}$_n$−) motifs are remarkably versatile building blocks for use in the assembly of polymetallic structures due to their unmatched ability to coordinate to metals in either σ- or π-fashion or a combination of both. In light of the diverse bonding modes available to polycarbon ligands it is hardly surprising that an equally diverse range of metal-containing groups has been attached to these ligands and there are many examples of complexes in which carbon molecules of various lengths are coordinated to multinuclear cluster frameworks.[13,14] However, most of the recent interest in the coordination chemistry of C_n ligands has been focused on structurally simpler complexes with greater potential for use in the realm of material

† University of Adelaide.
‡ Tel: +61 8 8303 5939. Fax: +61 8 8303 4358. E-mail: michael.bruce@adelaide.edu.au.
§ Present address: Department of Chemistry, University of Durham, South Road, Durham DH1 3LE, England.
|| Université de Rennes 1.
⊥ University of Melbourne.
Australian National University.

(1) Allen, G. C.; Hush, N. S. *Prog. Inorg. Chem.* **1967**, *8*, 357.
(2) Brown, D. M., Ed. *Mixed-Valence Compounds*; D. Reidel: Dordrecht, The Netherlands, 1980.
(3) Robin, M. B.; Day, P. *Adv. Inorg. Chem. Radiochem.* **1967**, *10*, 247.
(4) Taube, H. *Chem. Rev.* **1952**, *50*, 69.
(5) Haim, A. *Prog. Inorg. Chem.* **1983**, *30*, 273.
(6) For examples and lead references see: (a) Ung, V. A.; Cargill Thompson, A. M. W.; Bardwell, D. A.; Gatteschi, D.; Jeffery, J. C.; McCleverty, J. A.; Tolti, F.; Ward, M. D. *Inorg. Chem.* **1997**, *36*, 3447. (b) Cargill-Thompson, A. M. W.; Gatteschi, D.; McCleverty, J. A.; Navas, J. A.; Rentschler, E.; Ward, M. D. *Inorg. Chem.* **1996**, *35*, 2701.
(7) Ward, M. D. *Chem. Soc. Rev.* **1995**, 121.
(8) Long, N. J. *Angew. Chem., Int. Ed. Engl.* **1995**, *34*, 21.
(9) Whittall, I. R.; McDonagh, A. M.; Humphrey, M. G.; Samoc, M. *Adv. Organomet. Chem.* **1998**, *42*, 291; **1999**, *43*, 349.
(10) (a) *Atomic and Molecular Wires*; Joachim, C., Roth, S., Eds.; Kluwer: Dordrecht, The Netherlands, 1997. (b) *Molecular Electronics: Science and Technology*; Aviram, A., Ratner, M. A., Eds.; Annals of the New York Academy of Sciences, Vol. 852; New York Academy of Sciences: New York, 1998. (c) Diedrich, F.; Rubin, Y. *Angew. Chem.* **1992**, *104*, 1123; *Angew. Chem., Int. Ed. Engl.* **1992**, *31*, 1101. (d) Lang, H. *Angew. Chem.* **1994**, *106*, 569; *Angew. Chem., Int. Ed. Engl.* **1994**, *33*, 547. (e) Arnold, D. P.; Heath, G. A.; James, D. A. *New J. Chem.* **1998**, *22*, 1377. (f) Arnold, D. P.; Heath, G. A.; James, D. A. *J. Porphyrins Phthalocyanines* **1999**, *3*, 5.
(11) Paul, F.; Lapinte, C. *Coord. Chem. Rev.* **1998**, *178−180*, 431.
(12) (a) Frapper, G.; Kertesz, M. *Inorg. Chem.* **1993**, *32*, 732. (b) Osella, D.; Milone, L.; Nervi, C.; Ravera, M. *Eur. J. Inorg. Chem.* **1998**, 1473.

10.1021/ja992002t CCC: $19.00
Published on Web 02/17/2000

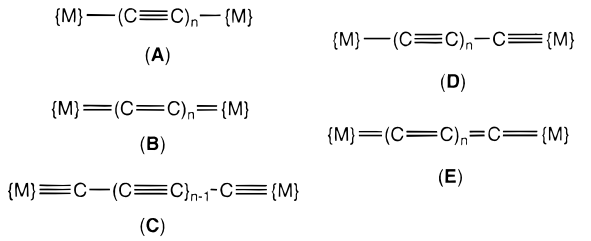

Figure 1. Valence-bond structures of all-carbon ligands bridging two metal centers.

science. The compounds $\{ML_x\}-C_n-\{M'L'_y\}$, in which the polycarbon chain is stabilized by interactions with just two metal centers form one such class. For even-numbered carbon chains, three configurations (excluding radical formulations) may be written (Figure 1, structures **A**−**C**). For compounds which feature an odd number of carbon atoms in the chain, at least one of the metal centers must be involved in an M−C multiple bond (Figure 1, structures **D** and **E**).

Experimentally, even-numbered carbon chains with predominantly polyyndiyl character (**A**) have been most commonly observed. However, it should be noted that through judicious choice of both metal−ligand combination and metal formal oxidation state, it has been possible to isolate examples of complexes with structures **A**, **B**, or **C**, e.g. for $n = 1$, $(Et_3P)_2ClPt-C\equiv C-Pt(PEt_3)_2$ (**A**),[16] $(Bu^tSiO)_3Ta=C=C=Ta(OSiBu^t_3)_3$ (**B**),[17] and $(Bu^tO)_3W-C\equiv C-W(OBu^t)_3$ (**C**).[18] Several intermediate structures associated with the presence of metal end-capping groups in dissimilar oxidation states[15,19,20] or electron-transfer processes[21] have also been reported. Recently, several subsets of these compounds have been subjected to high-level theoretical treatments in order to arrive at a more detailed description of their various electronic structures[12,15,17,19] In principle, structures **A**−**C** are related by a series of two-electron steps

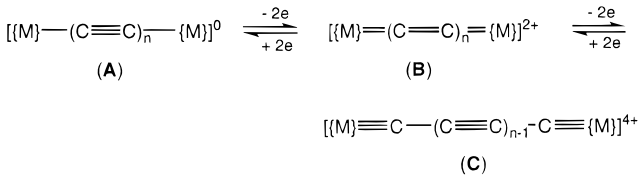

and the possibility that the complete range of structures **A**−**C** may be generated by oxidation of a single polyyndiyl complex (structure **A**) must therefore be considered.

While our initial studies in this area were concerned with the synthesis and reactivity of cluster-bound carbon molecules,[14] some of our more recent efforts have been directed toward a study of the synthesis and reactivity of complexes containing mononuclear metal fragments. We have described the preparation of the parent diynyl complexes $\{ML_n\}(C\equiv CC\equiv CH)$ and have demonstrated various methods by which the diynyl ligand may be elaborated to give both substituted diynyl complexes $\{ML_n\}(C\equiv CC\equiv CR)$ and diyndiyl complexes $\{L_nM\}(\mu\text{-}C\equiv CC\equiv C)\{M'L'_m\}$.[22]

The diyndiyl complexes $\{Cp^*(PPh_3)(NO)Re\}_2(\mu\text{-}C\equiv CC\equiv C)$ (**1**) and $\{Cp^*(dppe)Fe\}_2(\mu\text{-}C\equiv CC\equiv C)$ (**2**) have recently been

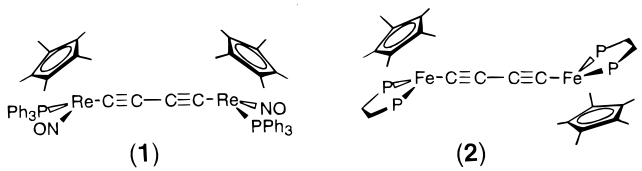

prepared and their oxidation chemistry explored by Gladysz[15] and Lapinte[20] and their respective co-workers. Both **1** and **2** undergo two reversible one-electron oxidation processes, evidenced by cyclic voltammetry. The large differences in the first two redox potentials for these complexes [$\Delta E° = 0.53$ (**1**), 0.72 V (**2**)] indicate that there are strong interactions between the metal centers. The metal centers in **1** are chiral, and both diastereomers of **1** have been oxidized by treatment with $AgPF_6$ in the appropriate stoichiometry to give the PF_6 salts of $[(SS/RR)\text{-}\mathbf{1}]^+$ and $[(SR/RS)\text{-}\mathbf{1}]^+$ and $[(SS/RR)\text{-}\mathbf{1}]^{2+}$ and $[(SR/RS)\text{-}\mathbf{1}]^{2+}$, with the retention of chirality at the metal centers in each case.[15] The oxidized species $[\mathbf{2}][PF_6]$ and $[\mathbf{2}][PF_6]_2$, containing the $\mathbf{2}^+$ and $\mathbf{2}^{2+}$ cations, respectively, have been obtained through chemical oxidation of **2** with 1 or 2 equiv of $[FcH][PF_6]$.[20]

While the carbon ligands in the neutral forms of both **1** and **2** have been shown to have 1,3-diacetylenic character (M−C≡CC≡C−M, **A**) through various combinations of crystallographic [Re−C 2.037(5), C≡C 1.202(7), C−C 1.389(5) Å[15]] and spectroscopic [ν(C≡C) 1968 w (**1**, KBr),[15] 1955 m and 1880 w (**2**, Nujol)[20]] methods, there appear to be significant differences in the nature of the carbon bridges in the oxidized forms $\mathbf{1}^+$ vs $\mathbf{2}^+$ and $\mathbf{1}^{2+}$ vs $\mathbf{2}^{2+}$. It has been established that there is a significant reduction in the C≡C bond order, with a corresponding increase in the C−C bond order, along the carbon bridge of **1** (Figure 1, structure **A**) upon oxidation to $\mathbf{1}^+$ and $\mathbf{1}^{2+}$. Crystallographic evidence indicates that the carbon ligand in $[\mathbf{1}][PF_6]_2$ is best described by a cumulenic structure (Figure 1, structure **B**).[15] In contrast, the spectral data from $\mathbf{2}^+$ (as well as crystallographic methods in this case) and $\mathbf{2}^{2+}$ are consistent with the retention of diacetylenic nature in the bridging C_4 ligand.[20] The unpaired electron in the monooxidized radical cation $\mathbf{1}^+$ is delocalized over both the metal centers and the C_4 chain; participation of the C_4 chain is not established in the case of $\mathbf{2}^+$.

More recently, Lapinte and his colleagues have reported a related study on the electron-rich complex $\{Cp^*(dippe)Fe\}_2(\mu\text{-}C_4)$ (dippe = $PPr^i_2CH_2CH_2PPr^i_2$) and the sequential chemical oxidation of this species by 2 equiv of $[FcH][PF_6]$ and 1 equiv of $AgPF_6$ to give the 33-electron species $[\{Cp^*(dippe)Fe\}_2(\mu\text{-}C_4)][PF_6]_3$.[23] On the basis of crystallographic data and ESR,

(13) See, for example: (a) Akita, M.; Moro-oka, Y. *Bull. Chem. Soc. Jpn.* **1995**, *68*, 420. (b) Koutsantonis, G. A.; Selegue, J. P.; Wang, J.-G. *Organometallics* **1992**, *11*, 2704. (c) Jensen, M. P.; Phillips, D. A.; Sabat, M.; Shriver, D. F. *Organometallics* **1992**, *11*, 1859. (d) Elder, S. M.; Robinson, B. H.; Simpson, J. *J. Organomet. Chem.* **1990**, *398*, 165. (e) Norton, D. M.; Stern, C. L.; Shriver, D. F. *Inorg. Chem.* **1994**, *33*, 2701.

(14) (a) Bruce, M. I. *J. Cluster Sci.* **1997**, *8*, 293. (b) Bruce, M. I. *Coord. Chem. Rev.* **1997**, *166*, 91. (c) Adams, C. J.; Bruce, M. I.; Horn, E.; Skelton, B. W.; Tiekink, E. R. T.; White, A. H. *J. Chem. Soc., Dalton Trans.* **1993**, 3299.

(15) Brady, M.; Weng, W.; Zhou, Y.; Seyler, J. W.; Amoroso, A. J.; Arif, A. M.; Bohme, M.; Frenking, G.; Gladysz, J. A. *J. Am. Chem. Soc.* **1997**, *119*, 775.

(16) Ogawa, H.; Onitsuka, K.; Joh, T.; Takahashi, S.; Yamamoto, Y.; Yamazaki, H. *Organometallics* **1988**, *7*, 2257.

(17) Neithamer, D. R.; LaPointe, R. E.; Wheeler, R. A.; Richeson, D. S.; Van Duyne, G. D.; Wolczanski, P. T. *J. Am. Chem. Soc.* **1989**, *111*, 9056.

(18) Listemann, M. L.; Schrock, R. R. *Organometallics* **1985**, *4*, 74.

(19) Belanzoni, P.; Nazzareno, R.; Sgamellotti, A.; Floriani, C. *J. Chem. Soc., Dalton Trans.* **1998**, 1825.

(20) Le Narvor, N.; Toupet, L.; Lapinte, C. *J. Am. Chem. Soc.* **1995**, *117*, 7129.

(21) Bruce, M. I.; Denisovich, L. I.; Low, P. J.; Peregudova, S. M.; Ustynyuk, N. A. *Mendeleev Commun.* **1996**, 200.

(22) (a) Bruce, M. I.; Ke, M.; Low, P. J. *Chem. Commun.* **1996**, 2405. (b) Bruce, M. I.; Ke, M.; Low, P. J.; Skelton, B. W.; White, A. H. *Organometallics* **1998**, *17*, 3539.

Scheme 1

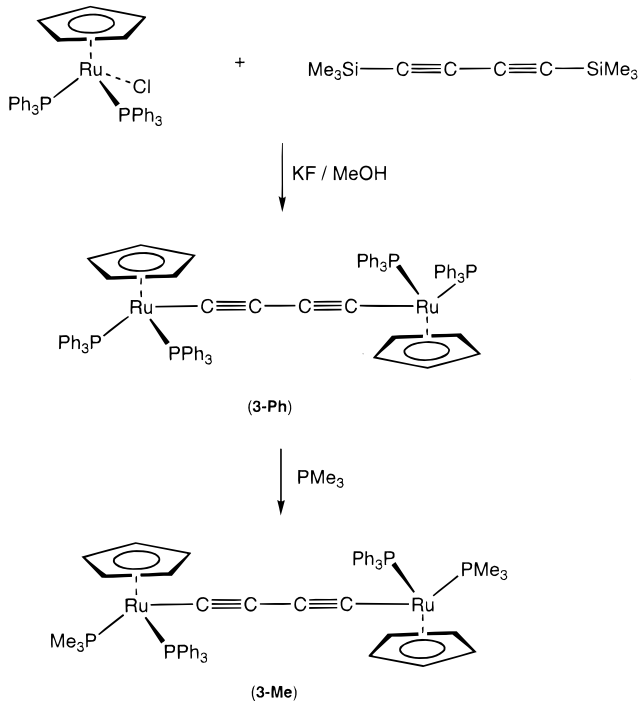

Mössbauer, and NIR spectroscopic evidence, a triradical structure featuring two Fe(III) centers and a carbon-centered radical has been proposed for the trication.

We now take the opportunity to describe the characterization of the complexes $[\{Cp(PPh_3)(PR_3)Ru\}_2(\mu\text{-}C{\equiv}CC{\equiv}C)]^{n+}$ [R = Ph (**3-Ph**), Me (**3-Me**); Cp = η^5-C_5H_5; $n = 0-4$] containing a bridging C_4 ligand which can be obtained in an unprecedented series of *five* oxidation states. A combination of chemical, spectroelectrochemical, and theoretical techniques have been employed to determine the nature of the C_4 ligand in each of these oxidation states. A preliminary account of some of this work has been published.[21]

Results

The known diacetylide-bridged diruthenium species $\{Cp(PPh_3)_2Ru\}_2(\mu\text{-}C{\equiv}CC{\equiv}C)$ (**3-Ph**) is more conveniently obtained in high yield from the reaction of $RuCl(PPh_3)_2Cp$ with 0.5 equiv of 1,4-bis(trimethylsilyl)buta-1,3-diyne, $Me_3SiC{\equiv}CC{\equiv}CSiMe_3$, in the presence of a source of fluoride ion.[24,26] Treatment of **3-Ph** with an excess of PMe_3 in refluxing toluene afforded the mixed phosphine complex $\{Cp(PPh_3)(PMe_3)Ru\}_2(\mu\text{-}C{\equiv}C\text{-}C{\equiv}C)$ (**3-Me**) in moderate yield (43%) (Scheme 1). The exchange of the PPh_3 ligands in $Ru(C{\equiv}CR)(PPh_3)_2Cp$ complexes for other ligands, particularly phosphines with smaller cone angles, has been well-documented.[25] The mixed phosphine complex **3-Me** was characterized by a single $\nu(C{\equiv}C)$ band in the IR spectrum at 1974 cm^{-1} and a parent ion at *m*/*z* 1056 in the electrospray (ES) mass spectrum. The fragment ions observed at higher cone voltages were also consistent with the proposed formulation and included $[Ru(PMe_3)(PPh_3)Cp]^+$ at *m*/*z* 505. A well-resolved singlet resonance was observed for the Cp ligands in both the ^1H (δ 4.43) and ^{13}C (δ 82.71) NMR spectra, while broad resonances associated with methyl groups of the PMe_3 ligands were observed in each case (δ_H 1.17, δ_C 22.50). A satisfactory microanalysis was also obtained.

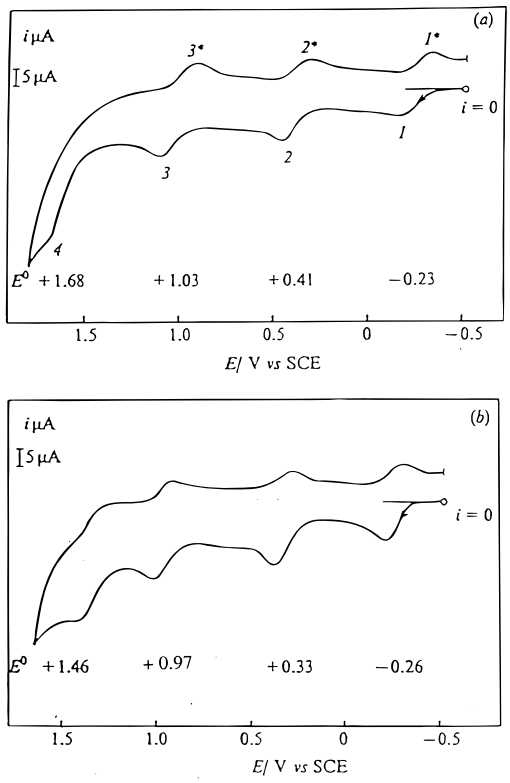

Figure 2. Cyclic voltammograms of **3-Ph** and **3-Me** (CH_2Cl_2, 0.1 M $[NBu_4][BF_4]$, 298 K, Pt working, counter and pseudo-reference electrodes). [**3-Ph** (**3-Me**): E°_1 −0.23 (−0.26); E°_2 +0.41 (+0.33); E°_3 +1.03 ($^+$0.97); $E^{3/4}_{pa} \approx E^\circ_4$ +1.68 ($^+$1.46) V].

In contrast to **3-Ph**, for which three rotamers have been crystallized to date,[24,26] it has not been possible to observe distinct rotamers of **3-Me** in either the solid state or in solution. Presumably the decreased steric bulk about each metal center in **3-Me**, compared with **3-Ph**, results in a much smaller degree of interaction between the ligand spheres and consequently less restricted rotation about the Ru−C(diyndiyl) bond. Furthermore, it should be borne in mind that both metal centers in **3-Me** are stereocenters and it is reasonable to suggest that **3-Me** exists as a mixture of diastereomers. The NMR spectra collected from samples of **3-Me** prepared as described above were free of any obvious line-doubling which might be expected to arise from the presence of both *RR*/*SS* and *RS*/*SR* enantiomeric pairs, as were the ν(CC) bands in the solid-state IR spectrum. The PMe_3 proton resonance was significantly broadened, although this may be attributable to the rotation processes indicated above rather than as an indication of the presence of diastereomers. Despite the success enjoyed by the Gladysz group in resolving *RR*/*SS* and *RS*/*SR* forms of **1**, exhaustive efforts to resolve samples of **3-Me** by fractional crystallization were unsuccessful. In the absence of single-crystal X-ray diffraction studies it is not possible to prove the absolute configuration at the metals in **3-Me**.

The cyclic voltammograms of **3-Ph** and **3-Me** were recorded at 298 K in CH_2Cl_2/0.1 M $[NBu_4][BF_4]$ and have been reported previously.[21] For convenience, these data are reproduced in Figure 2. In each case three quasi-reversible (ΔE_p = 100 mV) and one irreversible oxidation processes were observed, which are consistent with the oxidation of the neutral diyndiyl

(23) Guillemot, M.; Toupet, L.; Lapinte, C. *Organometallics* **1998**, *17*, 1928.
(24) Bruce, M. I.; Hall, B. C.; Kelly, B. D.; Low, P. J.; Skelton, B. K.; White, A. H. *J. Chem. Soc., Dalton Trans*. **1999**, 3719.
(25) Bruce, M. I.; Wong, F. S.; Skelton, B. W.; White, A. H. *J. Chem. Soc., Dalton Trans*. **1981**, 1398.
(26) Bruce, M. I.; Hinterding, P.; Tiekink, E. R. T.; Skelton, B. W.; White, A. H. *J. Organomet. Chem.* **1993**, *450*, 209.

Scheme 2

$$\textbf{3-Ph} + [\textbf{3-Ph}][PF_6]_2 \underset{}{\overset{K_c = 1.8 \times 10^{11}}{\rightleftharpoons}} 2\,[\textbf{3-Ph}][PF_6]$$

complexes in four steps. As would be expected for **3-Me** which contains the more electron-donating PMe_3 ligands, the formal potentials for this complex are significantly less positive than the corresponding redox processes in **3-Ph** (i.e. the oxidations of **3-Me** are thermodynamically more favorable than the corresponding oxidations of **3-Ph**). No reductions were observed within the solvent-imposed limit. The odd-electron species are thermodynamically stable with respect to disproportionation, as evidenced by the electrochemical data. For both **3-Ph** and **3-Me**, all the redox processes are well separated, with the differences in formal potentials, $\Delta E°$, lying in the range 0.49−0.65 V.

While the first three oxidation processes were confirmed as one-electron steps by comparison of the peak currents with that of an equimolar internal ferrocene standard, the irreversible fourth wave in the voltammogram appears to be a multielectron wave by comparison of the peak currents. This may be taken as an indication of the existence of an ECE mechanism in which the species $\mathbf{3}^{4+}$, once generated at the electrode surface, undergoes a rapid chemical transformation to a new species, which is then subject to a further oxidative process at the applied potential.

Chemical oxidation of **3-Ph** in dichloromethane with 1 equiv of $AgPF_6$ gave a deep green solution from which analytically pure [**3-Ph**][PF_6] was isolated as a dark green powder by precipitation into diethyl ether. The ES mass spectrum of [**3-Ph**][PF_6] was characterized by an intense $[\mathbf{3\text{-}Ph}]^+$ ion at *m*/*z* 1430. A strong ν(CC) band was observed at 1861 cm^{-1}, while the ν(PF) band from the counterion was observed at 840 cm^{-1}. Only broad featureless resonances were observed in the ^1H NMR spectrum of [**3-Ph**][PF_6] which suggests that the cation $[\mathbf{3\text{-}Ph}]^+$ is paramagnetic.

Oxidation of [**3-Ph**][PF_6] with a further 1 equiv of $AgPF_6$, or direct treatment of **3-Ph** with 2.5 equiv of the same oxidizing agent, afforded [**3-Ph**][PF_6]$_2$ as a dark blue microcrystalline solid following conventional workup and crystallization. In contrast to the monooxidized species, [**3-Ph**][PF_6]$_2$ gave well-resolved NMR spectra. The Cp ligands gave rise to single sharp resonances in both the ^1H (δ 5.03) and ^{13}C (δ 90.82) NMR spectra. Unfortunately the ^{13}C resonances from the carbon ligand could not be observed, even with long pulse delays. The ES mass spectrum of [**3-Ph**][PF_6]$_2$ at low cone voltages contained the intense doubly charged ion $[\mathbf{3\text{-}Ph}]^{2+}$ at *m*/*z* 715, with isotope peaks separated by 0.5 amu, consistent with the dicationic nature of this species. The ν(CC) band was observed at 1766 cm^{-1}.

The monooxidized species [**3-Ph**][PF_6] was also obtained from the comproportionation reaction of **3-Ph** with [**3-Ph**][PF_6]$_2$, as indicated in Scheme 2. It should also be noted that the CV of each of [**3-Ph**][PF_6] and [**3-Ph**][PF_6]$_2$ were identical with that of **3-Ph** measured under the same conditions. Unfortunately, all attempts to obtain [**3-Ph**][PF_6]$_3$ by further chemical oxidation were unsuccessful.

To collect more detailed information about the species detected by cyclic voltammetry, a series of spectroelectrochemical experiments was carried out, covering the IR, NIR, visible, and UV regions of the spectrum. The mid-IR spectra were collected in a modifed infrared reflection absorption spectroscopy (IRRAS) cell, while the samples for NIR/vis/UV spectroscopy were generated by electrolysis and analyzed in an optically transparent thin-layer electrode (OTTLE) cell in situ. Details of these experimental techniques have been given previously,[27,28] and only the particular details relevant to this work are described in the Experimental Section. In essence, the spectra of the various oxidized species were obtained from samples obtained by electrolysis of a small amount of solutions of **3** trapped in a thin film in the region about the working electrode. The working electrode was initially held at a resting potential at which the neutral complex was stable. Guided by the CV data, the applied potential was then increased to electrogenerate the monooxidized species $\mathbf{3}^+$. The reversiblity of the system under the conditions of the spectroelectrochemical experiment was confirmed by electrochemical reduction of the sample to give spectra identical to that of the precursor. The spectra of the higher oxidized species $\mathbf{3}^{n+}$ were obtained by similar processes of electrolysis, and reversibility was established by quantitative reduction to the precursor $\mathbf{3}^{(n-1)+}$ states.

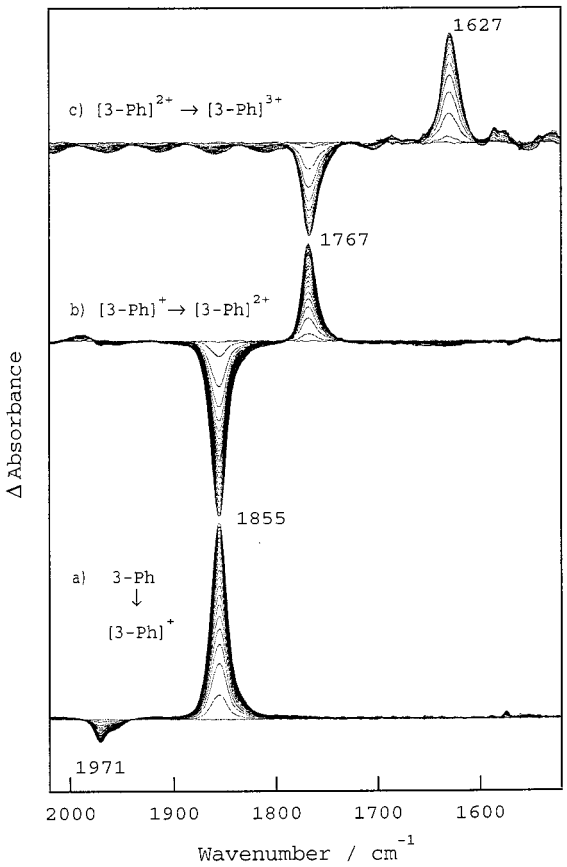

Figure 3. IR spectroelectrochemical spectra obtained following oxidation of **3-Ph**. The spectra were collected with a resolution of 4 cm^{-1} with time intervals of 1.6 s for (a) and (b) and 2.4 s for (c). In each case the reference spectrum was recorded immediately prior to the application of an oxidizing potential.

IR spectra recorded during the progressive oxidation of **3-Ph** and **3-Me** to their tricationic states are marked by a reduction in the wavenumber of ν(CC) (Figure 3 and Table 1). In keeping with their voltammetric response (Figure 2), oxidation and rereduction occur reversibly and on a similar time scale. Further oxidation to the tetracation is, at best, quasi-reversible, and oxidation of the trications was examined at temperatures of −40 °C or lower. Under these conditions we were unable to convert between the tri- and tetracations in the absence of significant concentrations of the dication. Indeed, the predominant transformation was between the di- and tetracations (Figure 4). The oxidation products, marked by a strong band at 1936 cm^{-1}, may

(27) (a) Best, S. P.; Clark, R. J. H.; McQueen, R. C. S.; Clooney, R. P. *Rev. Sci. Instrum.* **1987**, *58*, 2071. (b) Best, S. P.; Ciniawskii, S. A.; Humphrey, D. G. *J. Chem. Soc., Dalton Trans*. **1996**, 2945.

(28) Duff, C. M.; Heath, G. A. *Inorg. Chem.* **1991**, *30*, 2528.

Table 1. Mid-IR ν(CC) Absorptions (cm^{-1})

	$n = 0$	$n = 1$	$n = 2$	$n = 3$	$n = 4$
[**3-Ph**]$^{n+}$ [a]	1971, 1956	1855	1767	1627	1936
[**3-Me**]$^{n+}$ [a]	1972, 1957	1856	1767	1628	1928
1^{n+} [b]	1964	1872	not obsd		
2^{n+} [c]	1880, 1955	1880, 1973	1950, 2160		

[a] IRRAS, CH_2Cl_2 solution, 0.1 M [NBu^n_4][PF_6], −50 °C. [b] From ref 15. [c] From ref 20.

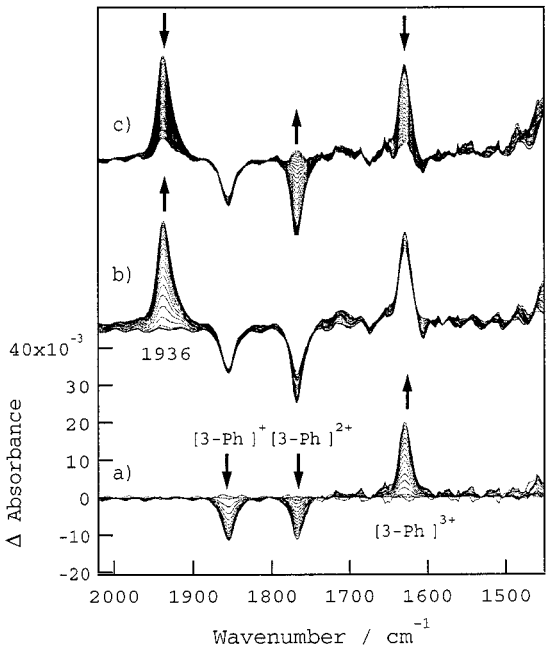

Figure 4. IR spectroelectrochemical spectra of **3-Ph** (initial potential = 0.72 V) obtained following the application of a potential of (a) 1.8, (b) 2.3, and (c) 0.72 V (spectral resolution = 4 cm^{-1}; time between spectra = 2.4 s).

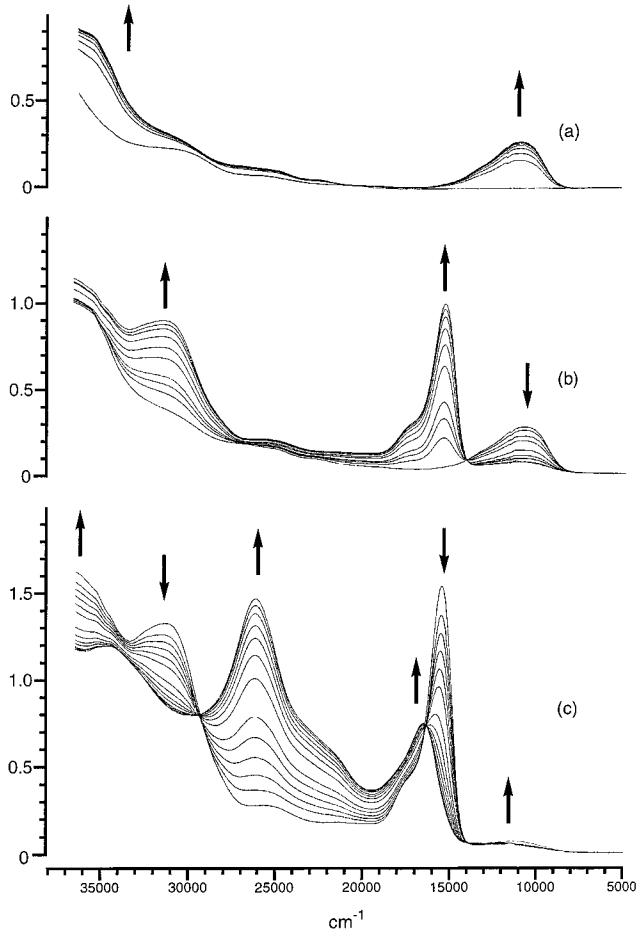

Figure 5. UV/vis/NIR spectra of (a) [**3-Ph**]$^{0/+}$, (b) [**3-Ph**]$^{+/2+}$, and (c) [**3-Ph**]$^{2+/3+}$ obtained from spectroelectrochemical experiments in an OTTLE cell (at −30 °C).

be rereduced with ca. 85% regeneration of the starting materials, although the rate of oxidation is markedly faster than that of rereduction (Figure 4b,c). Relatively large fluctuations in the baseline are evident in experiments leading to the generation of the tri- and tetracations, and this is likely to be due to the deposition of a solid film on the electrode.

The UV/vis/NIR spectroelectrochemical results are marked by similarly well-defined spectral changes, with clean isosbestic points marking the interconversions **3**/**3**$^+$, **3**$^+$/**3**$^{2+}$, and **3**$^{2+}$/**3**$^{3+}$ (Figure 5, Tables 2 and 3). Owing to the much longer time needed to perform the OTTLE experiments (ca. 8 min/scan) it was not possible to obtain spectra of **3**$^{4+}$.

Discussion

Several rotamers of **3-Ph** have been structurally characterized,[24,26] and these studies, in conjunction with the ν(C≡C) data reported both here and elsewhere[24,26] provide conclusive evidence that the structure of the carbon ligand in the neutral complex **3-Ph** is best described in terms of a 1,3-diacetylene type structure (Figure 6, structure **A**), as was observed for both the rhenium and iron complexes **1** and **2**.[15,20] Both metal centers in **3** may be regarded as formally Ru(II). The band due to ν(C≡C) in **3-Me** is similar to that of **3-Ph**, and the 1,3-diacetylenic structure may also be assigned to the C_4 ligand in **3-Me**.

Given the differences in the electronic structures of the C_4 bridges observed in the various oxidized forms of **1** and **2**, i.e., **1**$^+$ vs **2**$^+$ and **1**$^{2+}$ vs **2**$^{2+}$, the nature of the carbon ligands in the species formed by oxidation of **1** is of some interest. It should be noted at this point that the odd-electron species **3**$^+$ (35-e) and **3**$^{3+}$ (33-e) are both formally mixed-valence compounds and that no species corresponding to the quadruply-oxidized species **3**$^{4+}$ has yet been observed during the oxidation of either **1** or **2**.

The $\Delta E°$ values found for the redox processes reflect a large degree of electronic interaction between the metal centers through the C_4 bridge. Since the equilibrium constant, K_c, for the comproportionation reaction

$$[M^n]^+[M^{n+2}] \rightleftharpoons 2\,[M^{n+1}] \qquad (1)$$

is given by the expression[29]

$$K_c = [M^{(n+1)}]^2/[M^n][M^{(n+2)}] = \exp[\Delta E°(F/RT)] \qquad (2)$$

the electrochemical data allow the thermodynamic stabilities of the various oxidized species to be assessed.

The K_c values calculated for the odd-electron species **3**$^+$ ([**3-Ph**]$^+$, 1.5×10^{11}; [**3-Me**]$^+$, 2.1×10^{10}) and **3**$^{3+}$ ([**3-Ph**]$^{3+}$, 1.5×10^{11}; [**3-Me**]$^{3+}$, 2.7×10^8) are larger than has been found for the well-known Creutz−Taube ion {$Ru(NH_3)_5$}$_2$(μ-pyrazine) [$K_c = 10^{6.6}$ (aqueous solution),[30] $10^{7.3}$ (acetonitrile solution)[31]] and are comparable with the values previously reported for the related species [{Cp*(NO)(PPh_3)Re}$_2$(μ-C_4)]$^+$ (**1**$^+$) ($K_c = 3 \times 10^8$)[15] and [{Cp*(dppe)Fe}$_2$(μ-C_4)]$^+$ (**2**$^+$) ($K_c = 1.6 \times 10^{12}$).[20] The K_c values are large enough to allow the electrogenerated

(29) Richardson, D. E.; Taube, H. *Inorg. Chem.* **1981**, *20*, 1278.
(30) Creutz, C. *Prog. Inorg. Chem.* **1983**, *30*, 1.
(31) Creutz, C.; Chou, M. H. *Inorg. Chem.* **1992**, *31*, 3170.

Table 2. NIR IVCT Absorptions (cm^{-1})

	ν_{max} (cm^{-1})	ϵ (M^{-1} cm^{-1})	$\Delta\nu_{1/2}$ (obsd, cm^{-1})	$\Delta\nu_{1/2}$ (calcd from eq 3, cm^{-1})	H_{AB} [a] (eV)
[**3-Ph**]$^{+}$ [b]	11 400	8 000	3600	5131	0.71
[**3-Me**]$^{+}$ [c]	11 100	13 400	3200	5063	0.69
2^{2+} [d]	7 541	12 000	3250	4220	0.47
1^{3+} [e]	8 333	3 200	1500	4166	0.516
	10 000	9 400	1200	5000	0.620
	11 325	15 000	1800	5663	0.702
[**3-Ph**]$^{3+}$ [b]	12 200	900	3400	5308	0.76
[**3-Me**]$^{3+}$ [c]	12 000	1 700	3000	5264	0.74

[a] Also denoted V_{ab} in ref 17. [b] OTTLE cell, CH_2Cl_2 solution, 0.5 M [NBu^n_4][BF_4], −30 °C, sample concentration = 7.0×10^{-4} M. [c] OTTLE cell, CH_2Cl_2 solution, 0.5 M [NBu^n_4][BF_4], −30 °C, sample concentration = 2.3×10^{-3} M. [d] From ref 20. [e] From ref 15.

Table 3. UV−Vis Absorptions [λ_{max}, cm^{-1} (ϵ, M^{-1} cm^{-1})]

n	[**3-Ph**]$^{n+}$ [a]	[**3-Me**]$^{n+}$ [b]	**1**$^{n+}$ [c]	**2**$^{n+}$ [d]
0	32 200 (7140)	29 600 (5290)	28 902 (20 500)	
			37 037 (31 000)	
			43 104 (65 000)	
1	37 800 (27 700)	37 500 (50 500)	22 026 (6 400)	17 825 (700)
			28 735 (24 000)	22 883 (4100)
2	16 300 (45 400)	16 790 (47 700)	17 421 (30 000)	
	18 500 (11 700)	18 800 (15 900)	25 510 (41 000)	
	32 900 (38 600)	36 000 (49 300)	37 037 (25 000)	
			42 735 (57 000)	
3	17 300 (21 700)	18 450 (17 700)		
	27 500 (42 900)	29 500 (28 300)		
	36 400 (34 600)	37 000 (25 000)		

[a] OTTLE cell, CH_2Cl_2 solution, 0.5 M [NBu^n_4][BF_4], −30 °C, sample concentration = 7.0×10^{-4} M. [b] CH_2Cl_2 solution, 0.5 M [NBu^n_4][BF_4], −30 °C, sample concentration = 2.3×10^{-3}M. [c] From ref 15. [d] From ref 20.

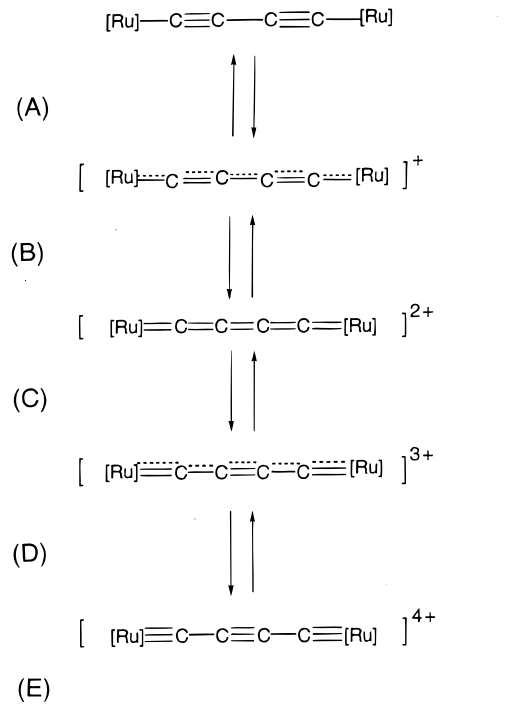

Figure 6. Elementary valence structures of **3**$^{n+}$ (n = 0−4).

species to be obtained as pure materials without any contamination from higher or lower oxidation states.

Both [**3-Ph**]$^{+}$ and [**3-Me**]$^{+}$ contain a single ν(CC) band approximately midway between the related neutral and dicationic species (Table 1). This observation provides strong evidence that the unpaired electron is delocalized over the molecule on the IR time scale (ca 10^{-12} s) and, consequently, that the metal centers in these odd-electron monocations **3**$^{+}$ are equivalent. A similar progression of ν(CC) to lower wavenumbers was observed for **1**, **1**$^{+}$, and **1**$^{2+}$.[15] Indeed, the similarity of the IR data for **1**$^{+}$ and **3**$^{+}$ suggests that the structure of the carbon ligand is similar in both cases. Each of the monocations **1**$^{+}$, **2**$^{+}$, and **3**$^{+}$ give rise to an IVCT band in the NIR region of the spectrum (Table 2) which is characteristic of the formally mixed-valence nature [M(II)/M(III)] of these compounds.[32] In the case of **3**$^{+}$ the position of ν_{max} was found to be virtually independent of solvent ([**3-Ph**]$^{+}$ 11 400 ± 50 (CH_2Cl_2), 11 300 ± 50 (MeCN); [**3-Me**]$^{+}$ 11 050 ± 50 cm^{-1} (CH_2Cl_2), 10 900 ± 50 cm^{-1} (MeCN)]. In addition, the widths of the IVCT bands at half-height ($\Delta\nu_{1/2}$) are considerably narrower than predicted from the relationship in eq 3 (Table 2),[30,32] which has been derived for complexes of class II in the well-known Robin−Day classification of mixed-valence systems.[3,33]

$$\Delta\nu_{1/2} = [2310\nu_{max}]^{1/2} \quad (3)$$

On the basis of all of the above data, it can be safely concluded that [**3-Ph**]$^{+}$ and [**3-Me**]$^{+}$ are Robin−Day class III "mixed-valence" compounds and that the unpaired electron is delocalized over the Ru−C_4−Ru six-atom fragment. The complexes are therefore best described as containing two Ru centers of intermediate oxidation state, rather than one localized Ru(II) center and one localized Ru(III) center. The energy of the IVCT band for class III complexes is related to the resonance energy between the ground and excited states, H_{AB}, by the expression[30,34,35]

$$H_{AB} = \nu_{max}/2 \quad (4)$$

The calculated values of H_{AB} are given in Table 2. These values

(32) Hush, N. S. *Prog. Inorg. Chem.* **1967**, *8*, 391.
(33) Astruc, D. *Electron Transfer and Radical Processes in Transition Metal Chemistry. Part 1*; VCH: New York, 1995.
(34) Woitelier, S.; Launay, J. P.; Spangler, C. W. *Inorg. Chem.* **1989**, *28*, 758.
(35) Dong, Y.; Hupp, J. T. *Inorg. Chem.* **1992**, *31*, 3170.

are large and as such are also entirely consistent with the class III description of these complexes. The complexes $\mathbf{3}^{+}$ may be therefore be described in terms of the series of simple valence bond forms represented by structure **B**, Figure 6. An alternative MO description is presented below.

Sharp, well-defined resonances were found in the ^{1}H NMR spectra of the isolated [**3-Ph**][PF_6]$_2$ complex, suggesting that the cation is diamagnetic. In terms of a model in which the oxidation processes are metal-based, this observation requires spin−spin coupling between two Ru(III) sites. An alternative model, in which the HOMO is not metal-centered but has appreciable carbon character as well, can also be invoked, and the diamagnetism of $\mathbf{3}^{2+}$ is then simply explained in terms of the removal of both electrons from this Ru−C_4−Ru derived HOMO and the return of the system to an $S = 0$ spin-paired ground state. Again, a more detailed discussion on this point is deferred to the Theoretical section below. However, it should be noted at this stage that the ν(CC) band is found at rather low frequency, suggesting a cumulenic structure (Figure 6, structure **C**) which, curiously, is more keeping with the nature of the rhenium complex $\mathbf{1}^{2+}$ than of the iron analogue $\mathbf{2}^{2+}$.[15,20]

The UV/vis spectra of [**3-Ph**]$^{2+}$ and [**3-Me**]$^{2+}$ are dominated by a new feature at 33 000 or 37 000 cm^{-1}, respectively, and intense transitions at 16 300 or 16 790 cm^{-1} (ϵ ca. 45 000 M^{-1} cm^{-1}), with smaller shoulders near 18 500 cm^{-1} in each case. There are no comparable bands found in the spectra of either **3** or $\mathbf{3}^{+}$, and therefore these features in the spectra of $\mathbf{3}^{2+}$ are most likely Ru−C(ligand) MLCT transitions.

The electrogenerated tricationic species $\mathbf{3}^{3+}$ are characterized by single, strong ν(CC) bands near 1627 cm^{-1}, the observation of which suggests a further decrease in the C≡C bond order in the C_4 bridge. In keeping with their formal mixed-valence Ru(IV)/Ru(III) composition, these species also give rise to characteristic NIR bands near 12 000 cm^{-1}, although the intensities of these bands are much less than those found for $\mathbf{3}^{+}$. In addition, MLCT bands were also observed (Figure 5c, Table 3). While the electrogenerated trications are thermodynamically ($K_c = 1.5 \times 10^{11}$, [**3-Ph**]$^{3+}$; 2.7×10^8, [**3-Me**]$^{3+}$) and kinetically stable in CH_2Cl_2 at −50 °C, attempts to generate [**3-Ph**]$^{3+}$ or [**3-Me**]$^{3+}$ in MeCN at low temperatures were complicated by the kinetic instability of these species in the more nucleophilic solvent. However, while the solvent dependence of these NIR bands cannot be easily assessed, assignment of $\mathbf{3}^{3+}$ as a class III Robin−Day system may still be made by noting that in addition to the single ν(CC) band and unique UV/vis spectra, the $\Delta\nu_{1/2}$ value is significantly smaller than the value calculated from eq 3 (Table 2). As was the case with $\mathbf{3}^{+}$ the values of H_{AB} calculated for $\mathbf{3}^{3+}$ from the NIR data are large ([**3-Ph**]$^{3+}$, 0.76 eV; [**3-Me**]$^{3+}$, 0.74 eV). These species may be described by structure **D** in Figure 6.

The quadruply-oxidized complexes $\mathbf{3}^{4+}$ are highly reactive and were only observed as transient species. The spectral changes associated with further oxidation of [**3-Ph**]$^{2+}$ are shown in Figure 4. In addition to the band associated with [**3-Ph**]$^{3+}$ an intense feature grows into the spectrum at 1936 cm^{-1}. Rereduction of this solution results in substantial regeneration of the starting products, indicating that the species responsible for the 1936 cm^{-1} band is chemically related to the starting material. The wavenumber of this feature is reminiscent of ν(CC) of an electron-deficient alkyne, and it is tempting to attribute to it the ν(CC) of the species indicated by structure **E** of Figure 6. This interpretation is unlikely, however, since for the approximately centrosymmetric complex the ν(CC) band for the central carbons of the bridge will contribute to the Raman-active modes and formally will be IR-inactive.

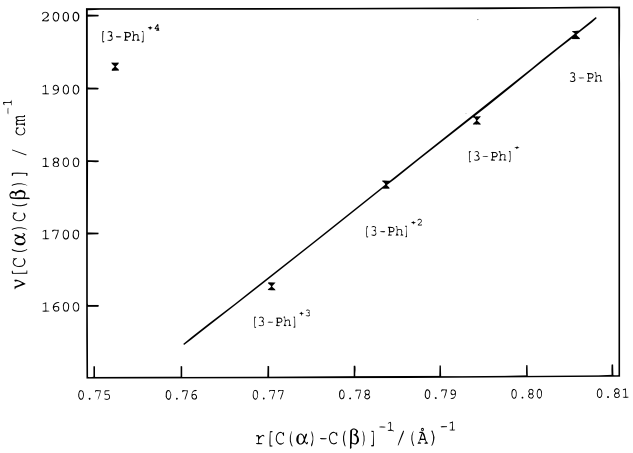

Figure 7. Plot of observed ν(CC) for [**3-Ph**]$^{n+}$ vs reciprocal of calculated C(α)−C(β) separations for [**3-H**]$^{n+}$ (Table 4).

A simple analysis of the linear Ru−C_α−C_β−C_β−C_α−Ru system shows that the stretching modes along the chain axis will result in three Raman, two infrared, and one translational mode. Provided that coupling between the Ru−C_α and C_α−C_β stretches is small, then the higher wavenumber IR-active stretching mode along the chain axis will be dominated by the C_α−C_β force constant. This being so, the wavenumber of the ν(CC) mode observed in the IR spectroelectrochemical experiments ought to correlate with the C_α−C_β force constant or, alternatively, the reciprocal of the C_α−C_β bond length. The DF calculations provide an estimate of this bond length (model **3-H**, Table 4), and an excellent linear correlation is obtained for the neutral through tricationic species (Figure 7). Thus both the wavenumber and intensity of the band obtained following further oxidation of $\mathbf{3}^{3+}$ are inconsistent with expectations based on structure **E**, Figure 6. Since the species responsible for the 1936 cm^{-1} band may, on a relatively rapid time scale, be reduced to generate **3**, it is unlikely that there is dissociation of the metal centers from the C_4 bridge. On the basis of the spectroscopy, either a highly asymmetric structure and/or diacetylenic character in the C_4 bridge may account for the 1936 cm^{-1} band. As mentioned above, this feature possibly arises from a complex formed by rapid oxidation of some species resulting from rapid chemical transformation of $\mathbf{3}^{4+}$; we defer speculating on the nature of this species until completion of further experiments.

Theoretical Analysis

To gain further insight into the electronic structure of the binuclear ruthenium diyndiyl species **3** and the structural and physical properties of the complexes formed upon oxidation, extended Hückel (EH) and density functional (DF) molecular-orbital calculations were carried out on the model complexes [{$Cp(PH_3)_2Ru$}$_2$(μ-C_4)]$^{n+}$, [**3-H**]$^{n+}$ ($n = 0-4$). Computational details are given in the Experimental Section.

Qualitative Analysis. We commence with an analysis of the neutral complex **3-H**. A simple EH molecular orbital diagram (Figure 8) is a useful aid in arriving at a qualitative understanding of the bonding between the C_4 chain and metallic end-caps. Using a fragment analysis, the formation of **3-H** can be envisioned as a result of the interaction of the frontier molecular orbitals (FMO) associated with the $(C_4)^{2-}$ unit with those of the bimetallic fragment [{$Ru(PH_3)_2Cp$}$_2$]$^{2+}$. The charges on the fragments have been chosen in such a way that the number of electrons associated with the carbon atoms of the C_4 fragment

Table 4. Selected Optimized Bond Lengths (Å) and Bond Angles (deg),[a] Relative Energies[b] (E_{rel}, eV), and Adiabatic Ionization Potentials[c] (IP, eV) for the Model Complexes $[\{Cp(PH_3)_2Ru\}_2(\mu\text{-}C_4)]^{n+}$, $[\mathbf{3\text{-}H}]^{n+}$, $[\{Cp^*(PH_3)_2Ru\}_2(\mu\text{-}C_4)]^{n+}$, $\mathbf{4}^{n+}$, $[\{Cp(dHpe)Ru\}_2(\mu\text{-}C_4)]^{n+}$, $\mathbf{5}^{n+}$, $[\{Cp^*(dHpe)Ru\}_2(\mu\text{-}C_4)]^{n+}$, $\mathbf{6}^{n+}$, $[\{Cp(CO)_2Ru\}_2(\mu\text{-}C_4)]^{n+}$, $\mathbf{7}^{n+}$, and $[\{Cp^*(CO)_2Ru\}_2(\mu\text{-}C_4)]^{n+}$, $\mathbf{8}^{n+}$, ($n = 0-4$)

model	Ru−C(α)	C(α)−C(β)	C(β)−C(β′)	Ru−C(α)−C(β)	C(α)−C(β)−C(β′)	E_{rel}	IP
3-H	2.022	1.241	1.367	176.3	176.9		
$[\mathbf{3\text{-}H}]^+$	1.968	1.259	1.335	176.5	176.8		4.83
$[\mathbf{3\text{-}H}]^{2+}$(LS)	1.923	1.276	1.314	179.5	176.0	0	8.65
$[\mathbf{3\text{-}H}]^{2+}$(HS)	1.915	1.279	1.310	178.8	175.7	0.10	8.75
$[\mathbf{3\text{-}H}]^{3+}$	1.880	1.298	1.291	179.6	175.6		12.28
$[\mathbf{3\text{-}H}]^{4+}$(LS)	1.853	1.329	1.271	177.7	176.5		16.37
4	2.030	1.243	1.388	176.3	177.0		
$\mathbf{4}^+$	1.974	1.260	1.339	176.4	176.7		4.53
$\mathbf{4}^{2+}$(LS)	1.932	1.274	1.316	176.8	176.5	0	8.10
$\mathbf{4}^{2+}$(HS)	1.929	1.279	1.314	177.2	176.3	0.15	8.25
$\mathbf{4}^{3+}$	1.898	1.294	1.294	177.4	176.2		11.59
$\mathbf{4}^{4+}$(LS)	1.884	1.310	1.289	178.5	176.4		15.18
5	2.028	1.241	1.369	176.4	176.8		
$\mathbf{5}^+$	1.973	1.258	1.339	176.1	177.2		4.63
$\mathbf{5}^{2+}$(LS)	1.926	1.275	1.317	176.0	177.3	0	8.41
$\mathbf{5}^{2+}$(HS)	1.918	1.281	1.311	176.2	177.2	0.05	8.46
$\mathbf{5}^{3+}$	1.886	1.301	1.292	176.1	177.4		12.01
$\mathbf{5}^{4+}$(LS)	1.850	1.333	1.276	176.5	177.1		15.95
6	2.039	1.244	1.371	176.8	176.5		
$\mathbf{6}^+$	1.986	1.260	1.341	177.6	176.2		4.34
$\mathbf{6}^{2+}$(LS)	1.934	1.275	1.319	177.5	176.2	0	7.86
$\mathbf{6}^{2+}$(HS)	1.931	1.282	1.314	177.9	176.0	0.14	8.00
$\mathbf{6}^{3+}$	1.900	1.297	1.296	177.9	175.9		11.30
$\mathbf{6}^{4+}$(LS)	1.873	1.320	1.281	179.8	179.9		14.89
7	2.037	1.231	1.367	176.0	177.3		
$\mathbf{7}^+$	1.992	1.252	1.334	175.6	177.4		6.48
$\mathbf{7}^{2+}$(LS)	1.949	1.270	1.310	176.4	176.7	0	10.74
$\mathbf{7}^{2+}$(HS)	1.948	1.277	1.304	176.5	176.6	−0.01	10.73
$\mathbf{7}^{3+}$	1.910	1.299	1.287	176.8	176.3		14.53
$\mathbf{7}^{4+}$(LS)	1.879	1.332	1.270	176.6	176.3		18.71
8	2.050	1.233	1.365	175.1	177.6		
$\mathbf{8}^+$	2.004	1.251	1.333	174.0	177.9		5.95
$\mathbf{8}^{2+}$(LS)	1.960	1.267	1.314	174.8	177.4	0	9.81
$\mathbf{8}^{2+}$(HS)	1.960	1.270	1.305	175.8	177.1	0.13	9.95
$\mathbf{8}^{3+}$	1.932	1.293	1.294	176.5	176.6		13.36
$\mathbf{8}^{4+}$(LS)	1.8	1.3	1.2	17	17		1

[a] Bonds lengths and bond angles are given for half of the molecule. Similar values are computed for the other half. [b] For low- (LS) and high-spin (HS) states. [c] IP = E(model$^+$) − E(model).

Scheme 3

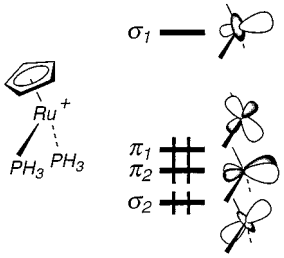

are consistent with the octet rule. The $(C_4)^{2-}$ moiety gives rise to sixteen MOs, six of which (two vacant and four occupied for the formal charge considered) may interact with the metallic fragment. These six FMOs, which are designated $1a_u$ and $2b_u$ (π^*), $2a_g$ (σ), $1b_g$ and $1a_g$ (π), and $1b_u$ (σ) under C_{2h} symmetry, are schematically sketched on the right-hand side of Figure 8. Each $Ru(PH_3)_2Cp$ metal fragment is a typical pseudo-ML_5 entity presenting a radial hybrid orbital (σ_1) situated above a "t_{2g}" set of d-type orbitals (π_1, π_2, σ_2) (see Scheme 3).[36] Consequently, the binuclear ruthenium fragment exhibits a set of eight FMOs which span $3b_u$ and $3a_g$ (out-of-phase and in-phase combinations of the hybrid FMO σ_1), $2b_u$ and $2a_g$ (out-of-phase and in-phase combinations of the d-type FMO π_1), $1a_u$ and $1b_g$ (out-of-phase and in-phase combinations of the d-type FMO π_2), and $1b_u$ and $1a_g$ (out-of-phase and in-phase combinations of the d-type FMO σ_2) under C_{2h} symmetry.

For the neutral species **3-H**, the bonding between the metallic and the carbon fragments is mainly governed by strong σ-type interactions occurring between the high-lying metallic FMOs $3b_u$ and $3a_g$ and the low-lying C_4 orbitals $1b_u$ and $2a_g$ which lead to an important electron donation from the C_4 spacer toward the metallic fragment. The degree of electron donation is illustrated numerically by the braced digits in Figure 8 which indicate the electron occupation of FMOs following the interaction of the component fragments. The σ-type M−C bonding is complemented by a rather weak π-type back-donation from occupied metallic FMOs into the high-lying acceptor C_4 FMOs $1a_u$ and $2b_u$. The electron occupation of these orbitals is calculated to be 0.20 and 0.22, respectively. The large energy difference between the donor metallic FMOs and the acceptor orbitals on the C_4 fragments limits the degree to which these back-bonding interactions may contribute to the M−C bonding in **3-H** and related compounds.[37] The predominant M−C π-type interactions are actually filled/filled interactions between the occupied carbon and metal π orbitals, in particular between the $1b_g$ and $1a_g$ FMOs of the C_4 bridge and the corresponding occupied metallic FMOs with the same symmetry ($1b_g$ and $2a_g$). As a result of these interactions, the C_4 orbitals are stabilized, while the metallic orbitals are destabilized and become the

(36) Schilling, B. E. R.; Hoffmann, R.; Lichtenberger, D. L. *J. Am. Chem. Soc.* **1979**, *101*, 585.

(37) Lichtenberger, D. L.; Renshaw, S. K.; Wong, A.; Tagge, C. D. *Organometallics* **1993**, *12*, 3522.

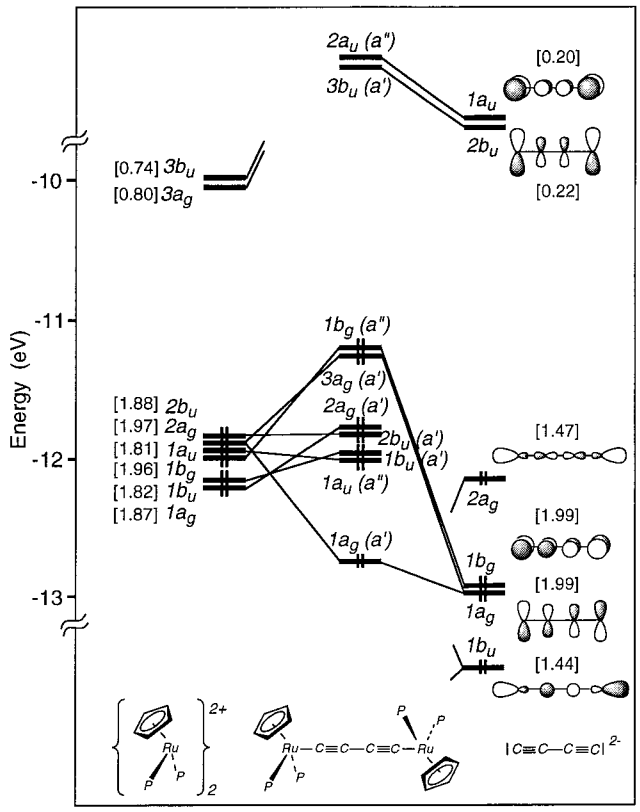

Figure 8. EH orbital interaction diagram for the neutral model complex [{Cp(PH$_3$)$_2$Ru}$_2$(μ-C$_4$)] (**3-H**) of C_{2h} symmetry (labels in the C_s symmetry group in parentheses). FMO occupations after interaction are given in brackets.

HOMOs of the neutral system. An important consequence of these π-type interactions is the mixing of the C_4 and Ru_2 FMOs which leads to a large percentage contribution from the carbon atoms of the C_4 unit to the HOMOs of **3-H** (53% ruthenium and 32% C_4, and 64% ruthenium and 29% C_4 in character for $1b_g$ and $2a_g$, respectively). The HOMOs are therefore delocalized over the entire six-atom Ru−C_4−Ru chain, and it may be concluded that any oxidation process which involves loss of electrons from these orbitals will not be exclusively metal-centered. Since the HOMOs are antibonding between Ru and C(α) and between C(β) and C(β'), but bonding between C(α) and C(β), the computational work suggests that shortening of the M−C and C−C single bonds and lengthening of the C≡C triple bonds are to be expected upon oxidation of **3-H**.

In addition, it should be noted that the HOMOs are well separated from the high-lying LUMOs $2a_u$ and $3b_u$ (3.37 eV) and are also removed from the other occupied metallic MOs, as illustrated in the middle of Figure 8. Therefore **3-H** should be capable of losing up to four electrons and give rise to a series of five oxidation states, as was observed experimentally for **3-Ph** and **3-Me**.

These qualitative conclusions are supported further by density functional molecular-orbital calculations, which were carried out on the model complexes [**3-H**]$^{n+}$ (n = 0−4). Partial density functional optimization on [**3-H**]$^{n+}$ was made under the C_s symmetry constraint in order to reduce computational effort. C_s symmetry (with the σ_h plane bisecting the Cp ligands and containing the Ru−C_4−Ru chain) instead of C_{2h} symmetry was chosen for the models in order to differentiate the ruthenium centers.

Bond Distances. Pertinent results of DF geometry optimization on [**3-H**]$^{n+}$ (n = 0−4) species are shown in Table 4. The C_s model **3-H** quite satisfactorily mimics the atomic distances of the crystallographically characterized complex {Cp(PPh$_3$)$_2$Ru}$_2$(μ-C≡CC≡C), **3-Ph**. The computed Ru−C(α), C(α)−C(β), and C(β)−C(β') distances for **3-H** are 0.030 Å longer, 0.016 Å longer, and 0.010 Å shorter than observed for the *trans*-isomer of **3-Ph**, which is the most accurately characterized rotamer to date.[26] The small deviations of the computed distances from the experimental values may be ascribed to some extent by the partial optimization and the different substituents, PH_3 in **3-H** vs. PPh_3 in **3-Ph**. The computed Ru−C(α)−C(β) and C(α)−C(β)−C(β') angles (176.3 and 176.9°) are reproduced at remarkably high accuracy with deviations of 1.3 and 0.1°, respectively, from the experimental values. The good agreement between metric parameters computed for **3-H** and the corresponding experimental values obtained from **3-Ph** gives confidence in the computed bond distances in [**3-H**]$^{n+}$ cations for which no X-ray data are available yet.

As expected from the qualitative EH approach discussed above, the atomic distances in the Ru−C_4−Ru chain of [**3-H**]$^{n+}$ were found to vary following the sequential removal of electrons (Table 4). For instance, upon oxidation of **3-H** to [**3-H**]$^{2+}$ the Ru−C(α) and C(β)−C(β') bonds contract by 0.099 (5%) and 0.053 Å (4%), respectively, whereas the C(α)−C(β) bond lengthens by 0.035 Å (3%). Similarly, upon oxidation from [**3-H**]$^{2+}$ to [**3-H**]$^{4+}$ the Ru−C(α) and C(β)−C(β') bonds shorten by a further 0.070 (4%) and 0.043 Å (3%), respectively, while the C(α)−C(β) bond lengthens by 0.053 Å (4%). Larger changes in Re−C and C−C bond lengths were computed between the rhenium analogues {Cp*(PPh$_3$)(NO)Re}$_2$(μ-C$_4$) and [{Cp*(PPh$_3$)(NO)Re}$_2$(μ-C$_4$)]$^{2+}$.[15] Nevertheless the changes in the bond lengths computed as the oxidation of **3-H** proceeds seem to indicate a conversion of the neutral diyndiyl model complex **3-H** (Figure 6, structure **A**) through the dicarbenic species [**3-H**]$^{2+}$ (Figure 6, structure **C**) into an acetylene-bridged dicarbyne complex [**3-H**]$^{4+}$ (Figure 6, structure **E**). For illustration, the computed Ru−C bond length in [**3-H**]$^{4+}$ (1.85 Å) is somewhat longer than Os≡C separations (ca 1.78 Å) observed in osmium−carbyne complexes (no Ru≡C distances have been structurally determined at present).[38] The gradual decrease in bond order along the carbon chain is consistent with the bond stretching frequencies [ν(CC)] measured experimentally (Table 1, Figure 6). In addition, it is noteworthy that C−C distances computed for [**3-H**]$^{3+}$ compare rather well with the corresponding C−C distances determined experimentally for the tricationic diiron species [{Cp*(dippe)Fe}$_2$(μ-C$_4$)]$^{3+}$.[23]

One of the puzzling features associated with the spectral data for [**3-Ph**]$^{2+}$ and [**3-Me**]$^{2+}$ lies in the apparent cumulenic structure of the carbon chain, which, as has been indicated above, is more in keeping with the nature of the rhenium complex **3**$^{2+}$ than of the iron analogue **2**$^{2+}$. On the basis of the Mössbauer spectroscopic data, a high-spin diacetylenic diradical $^{+\bullet}$Fe−C≡C−C≡C−Fe$^{\bullet+}$ valence formulation for **2**$^{2+}$ with Fe(III) termini has been proposed.[20] In an effort to address this issue, spin-unrestricted calculations were carried out on the model complex [**3-H**]$^{2+}$. The results indicated no significant differences between the bond lengths optimized for the high-spin (HS) and low-spin (LS) configurations. The largest deviation was found in the Ru−C(α) separation, which is 0.008 Å longer in the LS configuration than in the HS configuration. Comparable results were obtained from both HS and LS configurations of the doubly charged diiron model compound

(38) (a) Clark, G. R.; Marsden, K.; Roper, W. R.; Wright, L. J. *J. Am. Chem. Soc.* **1980**, *102*, 6570. (b) Clark, G. R.; Edmonds, N. R.; Pauptit, R. A.; Roper, W. R.; Waters, J. M.; Wright, A. H. *J. Organomet. Chem.* **1983**, *244*, C57.

Table 5. Energies (ϵ, eV) and Metal and C_4 Percentage Compositions of Selected Orbitals in the HOMO/LUMO Region of $[\{Cp(PH_3)_2Ru\}_2(\mu\text{-}C_4)]^{n+}$, $[\mathbf{3\text{-}H}]^{n+}$ ($n = 0-4$)

		MO							
		23a″	36a′	22a″	35a′	21a″	34a′	33a′	32a′
[3-H]	ϵ	−1.18	−1.22	−3.00	−3.20	−4.35	−4.50	−4.61	−4.83
	occ	0	0	2	2	2	2	2	2
	M	42	16	27	25	59	67	63	74
	C_4	0	0	59	69	15	11	7	11
	Cp	35	2	8	2	15	14	20	7
	$(PH_3)_2$	33	82	5	4	11	7	9	8
$[\mathbf{3\text{-}H}]^+$	ϵ α)	−4.37	−4.02	−6.85	−6.89	−8.04	−7.93	−7.99	−8.35
	$\epsilon(\beta)$	−4.32	−4.00	−6.48	−6.81	−7.86	−7.87	−7.92	−8.28
	occ(α/β)	0/0	0/0	1/0	1/1	1/1	1/1	1/1	1/1
	M(α/β)	41/41	14/14	32/32	34/34	56/56	63/63	61/61	78/78
	C_4(α/β)	0/0	2/2	52/52	61/61	15/15	9/9	6/6	11/11
	Cp(α/β)	27/27	4/4	9/9	2/2	18/18	20/20	23/23	5/5
	$(PH_3)_2$ (α/β)	32/32	79/79	6/6	3/3	11/11	8/8	10/10	7/7
$[\mathbf{3\text{-}H}]^{2+}$(LS)	ϵ	−7.63	−7.18	−10.30	−10.44	−11.59	−11.36	−11.37	−11.91
	occ	0	0	0	2	2	2	2	2
	M	40	31	36	38	46	55	54	77
	C_4	0	37	44	56	15	10	7	11
	Cp	28	23	12	3	25	25	28	5
	$(PH_3)_2$	32	9	8	3	14	10	11	6
$[\mathbf{3\text{-}H}]^{2+}$ (HS)	ϵ(α)	−7.68	−7.48	−10.48	−10.92	−11.67	−11.42	−11.43	−12.20
	$\epsilon(\beta)$	−7.57	−7.19	−10.07	−10.40	−11.45	−11.29	−11.30	−11.93
	occ(α/β)	0/0	0/0	1/0	1/0	1/1	1/1	1/1	1/1
	M(α/β)	40/40	28/28	37/37	38/38	48/48	57/57	57/56	77/76
	C_4(α/β)	0	41/41	44/44	57/56	16/16	8/8	6/6	12/12
	Cp(α/β)	28/28	21/21	11/11	3/3	23/23	25/25	26/27	5/6
	$(PH_3)_2$ (α/β)	32/32	10/10	8/8	3/3	13/13	10/9	10/10	6/6
$[\mathbf{3\text{-}H}]^{3+}$	ϵ(α)	−11.00	−11.15	−13.93	−14.46	−15.18	−14.83	−14.85	−15.78
	$\epsilon(\beta)$	−10.95	−10.80	−13.85	−14.03	−15.15	−14.77	−14.78	−15.59
	occ(α/β)	0/0	0/0	0/0	1/0	1/1	1/1	1/1	1/1
	M(α/β)	38/38	19/19	37/37	39/39	33/33	49/49	49/49	73/73
	C_4(α/β)	0/0	62/63	39/39	56/55	15/15	8/8	8/8	12/12
	Cp(α/β)	28/28	13/13	14/14	3/3	34/34	32/32	32/32	7/8
	$(PH_3)_2$ (α/β)	33/33	5/5	10/10	2/2	17/17	11/11	11/11	7/6
$[\mathbf{3\text{-}H}]^{4+}$ (LS)	ϵ	−14.73	−14.98	−17.44	−18.04	−19.66	−18.23	−18.26	−19.41
	occ	0	0	0	0	2	2	2	2
	M	13	13	35	41	21	42	43	64
	C_4	76	79	35	52	14	7	10	10
	Cp	7	6	18	5	43	38	35	17
	$(PH_3)_2$	3	1	12	2	21	12	12	8

$[\{Cp(PH_3)_2Fe\}_2(\mu\text{-}C_4)]^{2+}$, which was used to mimic the complex $[\{Cp^*(dppe)Fe\}_2(\mu\text{-}C_4)]^{2+}$ ($\mathbf{2}^{2+}$).[39] Clearly, some care must be taken in assigning cumulenic or acetylenic forms to complexes such as $[\mathbf{3\text{-}H}]^{2+}$ on the basis of bond lengths alone.

MO Analysis. The density-functional molecular orbital diagram of the neutral model **3-H** shown in Figure 9 is qualitatively similar to the EHMO diagram given in Figure 8. A large energy gap separates the occupied and vacant orbital sets (1.78 eV), as expected for complexes containing 18-electron metal centers. It is informative to look at the energy and composition of the orbitals located in the HOMO region in order to better discuss the structural trends observed for **3-H** upon oxidation. To this end, a Mulliken atomic orbital population analysis for selected MOs is given in Table 5. The 22″ and 35a′ orbitals, which are the HOMOs for the neutral species **3-H**, are delocalized along the Ru−C_4−Ru chain and feature an appreciable component from C_4 moiety. The 22a″ level is 27% metal and 59% C_4 in character, whereas the 35a′ orbital contains 25% metal and 69% C_4 character. The contour plots of the HOMOs are illustrated in Figure 10 and confirm the EH results discussed above; i.e., these MOs are π-type in character and antibonding between Ru and C(α) and C(β) and C(β') and bonding between C(α) and C(β). They extend perpendicularly to each other. The composition of these orbitals is not significantly altered upon oxidation, and they remain essentially delocalized over the six-atom Ru_2C_4 core, although there is a small increase in the amount of metal character and a corresponding decrease in the C_4 content during the progression from **3-H** to $[\mathbf{3\text{-}H}]^{4+}$ (Table 5). Thus, the bond length variations

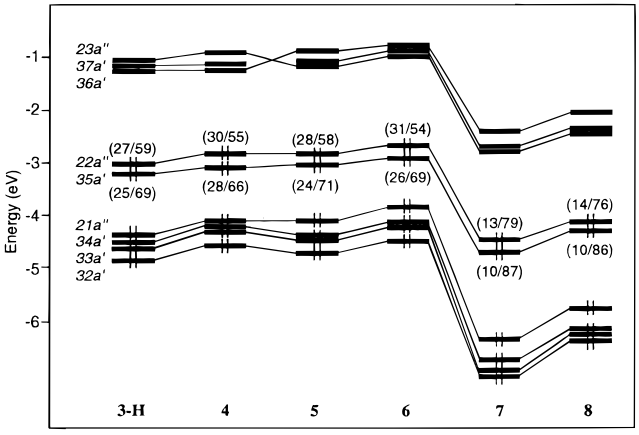

Figure 9. DF orbital diagrams for the neutral model complexes $\{Cp(PH_3)_2Ru\}_2(\mu\text{-}C_4)$ (**3-H**), $\{Cp^*(PH_3)_2Ru\}_2(\mu\text{-}C_4)$ (**4**), $\{Cp(dHpe)Ru\}_2(\mu\text{-}C_4)$ (**5**), $[\{Cp^*(dHpe)Ru\}_2(\mu\text{-}C_4)$ (**6**), $\{Cp(CO)_2Ru\}_2(\mu\text{-}C_4)$ (**7**), and $\{Cp^*(CO)_2Ru\}_2(\mu\text{-}C_4)$ (**8**) of C_s symmetry. The metal/carbon percentage contributions to HOMOs are given in parentheses.

(39) Costuas, K.; Halet, J.-F.; Lapinte, C. Unpublished results, 1999.

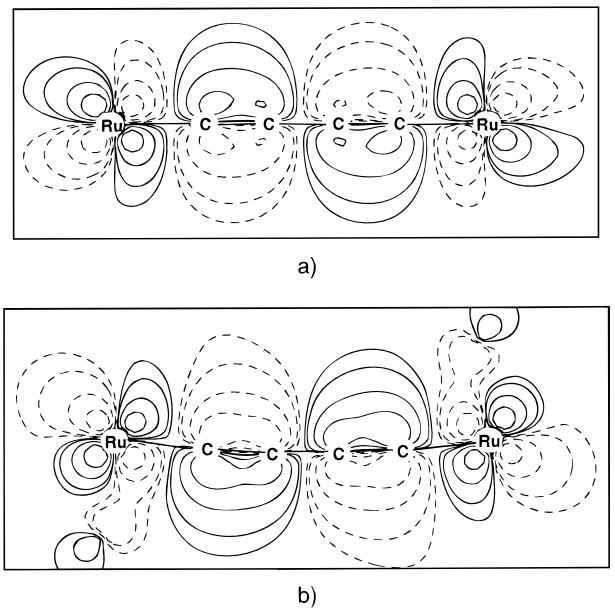

Figure 10. Contour plots of (a) the 22a″ MO (in the plane bisecting the Cp ligands) and (b) the 35a′ MO [in a plane perpendicular to that in (a)] HOMOs of the neutral model complex $\{Cp(PH_3)_2Ru\}_2(\mu\text{-}C_4)$ (**3-H**). Contour values are ±0.01, ±0.02, ±0.05, ±0.1, ±0.2, and ±0.5 $(e/bohr^3)^{1/2}$.

computed upon oxidation (Table 4) are in agreement with the notion of removal of electrons from these MOs. As both 22a″ and 35a′ MOs have the same bonding/antibonding character along the Ru−C_4−Ru chain, it is not surprising that the Ru−C and C−C bond lengths computed for the model complex $[\mathbf{3\text{-}H}]^{2+}$ are essentially identical for either the LS $(35a')^2(22a'')^0$ or HS $(35a')^1(22a'')^1$ electronic configurations (Table 4). Furthermore, regardless of the charge on the model complex $[\mathbf{3\text{-}H}]^{n+}$, the two 35a′ and 22a″ MOs remain largely separated in energy from the higher vacant MOs and are also separated, to a lesser extent, from the low-lying occupied MOs which are mainly metallic in character (Table 5). The evolution of the atomic net charges computed in the different models $[\{Cp(PH_3)_2Ru\}_2(\mu\text{-}C_4)]^{n+}$ according to the Hirshfeld analysis[40,41] confirms the delocalized character of the 35a′ and 22a″ MOs, and both metal and carbon atoms lose electron density upon oxidation (Table 6).

In accord with the diamagnetism observed for the dicationic ruthenium species $[\mathbf{3\text{-}Ph}]^{2+}$, the singlet state associated with the $(35a')^2(22a'')^0$ electronic configuration of $[\mathbf{3\text{-}H}]^{2+}$ is preferred by 0.1 eV (9.6 kJ/mol) over the triplet state which is associated with the $(35a')^1(22a'')^1$ electronic configuration for the same model complex. The singlet state associated with the $(21a'')^2(35a')^0$ electronic configuration is largely energetically favored compared to the triplet state associated with the $(21a'')^1(35a')^1$ electronic configuration for the tetracationic species $[\mathbf{3\text{-}H}]^{4+}$.

With respect to the iron-based analogues such as **2**, it should also be noted that on the basis of CV evidence it has been concluded that the iron−iron interaction across the C_4 bridge becomes greater as the electron density on the metal centers increases.[23] This observation may be taken as a qualitative indication of an increase in the amount of carbon character in

(40) In contrast to the Mulliken population analysis, the Hirschfeld method yields atomic charges which are essentially stable against basis sets variations and correctly reflect the electronegativity differences between the atoms. See for example: Bickelhaupt, F. M.; van Eikama Hommes, N. J. S.; Guerra, C. F.; Baerends, E. J. *Organometallics* **1996**, *15*, 2923.

(41) Hirshfeld, F. L. *Theor. Chem.* **1977**, *44*, 129.

Table 6. Averaged Computed Hirshfeld Charges of Selected Atoms in the Complex Models $[\{Cp(PH_3)_2Ru\}_2(\mu\text{-}C_4)]^{n+}$, $[\mathbf{3\text{-}H}]^{n+}$, $[\{Cp^*(PH_3)_2Ru\}_2(\mu\text{-}C_4)]^{n+}$, $\mathbf{4}^{n+}$, $[\{Cp(dHpe)Ru\}_2(\mu\text{-}C_4)]^{n+}$, $\mathbf{5}^{n+}$, $[\{Cp^*(dHpe)Ru\}_2(\mu\text{-}C_4)]^{n+}$, $\mathbf{6}^{n+}$, $[\{Cp(CO)_2Ru\}_2(\mu\text{-}C_4)]^{n+}$, $\mathbf{7}^{n+}$, and $[\{Cp^*(CO)_2Ru\}_2(\mu\text{-}C_4)]^{n+}$, $\mathbf{8}^{n+}$ ($n = 0-4$)

	n charge				
	0	1	2[a]	3	4[a]
			Ru		
3-H	0.157	0.189	0.234	0.282	0.332
4	0.165	0.197	0.236	0.279	0.321
5	0.158	0.191	0.235	0.281	0.331
6	0.170	0.201	0.241	0.281	0.324
7	0.336	0.362	0.406	0.449	0.499
8	0.342	0.365	0.401	0.434	
			C(α)		
3-H	−0.239	−0.169	−0.121	−0.068	−0.021
4	−0.230	−0.168	−0.127	−0.081	−0.048
5	−0.241	−0.172	−0.126	−0.069	−0.024
6	−0.232	−0.171	−0.132	−0.083	−0.046
7	−0.207	−0.105	−0.049	0.018	0.070
8	−0.201	−0.111	−0.068	−0.011	
			C(β)		
3-H	−0.140	−0.080	−0.030	0.024	0.075
4	−0.137	−0.083	−0.039	0.007	0.041
5	−0.142	−0.083	−0.034	0.021	0.071
6	−0.139	−0.086	−0.043	0.004	0.044
7	−0.097	−0.020	0.036	0.095	0.146
8	−0.099	−0.030	0.016	0.064	

[a] Low-spin configuration.

the HOMOs of the complex featuring the more electron-rich iron termini due to an increase in the interactions between the filled metal fragment and carbon-chain π-type orbitals similar to those described above for **3-H**. Interestingly enough, HOMOs computed for the model complex $\{Cp(PH_3)_2Fe\}_2(\mu\text{-}C_4)$ are much more metallic in nature than their corresponding MOs in complex **3-H** (38% and 33% vs 27% and 25% in MO 22a″ and MO 35a′, respectively)[39] which presumably contributes to the metal-centered diradical character of the dioxidized complex $\mathbf{2}^{2+}$. Concomitantly, the participation of the C_4 chain is smaller in the former than in the latter (51% and 61% vs 59% and 69% in MO 22a″ and MO 35a′, respectively).[39] Consequently, the iron atoms are slightly negatively charged, whereas the ruthenium atoms are slightly positively charged, and the carbon atoms of the C_4 chain are slightly less electron-rich in the iron species than in the ruthenium species. Furthermore, in contrast to $[\mathbf{3\text{-}H}]^{2+}$ similar energies are computed for both HS and LS configurations for the iron model $[\mathbf{2\text{-}H}]^{2+}$ in accord with the very weak antiferromagnetic coupling observed for $\mathbf{2}^{2+}$ at low temperature.[20,39] The singlet−triplet energy difference is sufficiently small to render $\mathbf{2}^{2+}$ paramagnetic at liquid nitrogen temperature.[20]

Electronic Influence of the Surrounding Ligands. To estimate the change in the electronic structure of **3-H** induced by various modifications of the donor/acceptor properties associated with the surrounding ligands, DF calculations were carried out on different models in which the Cp and PH_3 ligands of **3-H** were substituted by Cp* and CO or $PH_2CH_2CH_2PH_2$ (dHpe), respectively. Selected structural parameters resulting from the geometry optimizations of the complexes $[\{Cp^*(PH_3)_2Ru\}_2(\mu\text{-}C_4)]^{n+}$, $\mathbf{4}^{n+}$, $[\{Cp(dHpe)Ru\}_2(\mu\text{-}C_4)]^{n+}$, $\mathbf{5}^{n+}$, $[\{Cp^*(dHpe)Ru\}_2(\mu\text{-}C_4)]^{n+}$, $\mathbf{6}^{n+}$, $[\{Cp(CO)_2Ru\}_2(\mu\text{-}C_4)]^{n+}$, $\mathbf{7}^{n+}$, and $[\{Cp^*(CO)_2Ru\}_2(\mu\text{-}C_4)]^{n+}$, $\mathbf{8}^{n+}$ ($n = 0-4$), are compared in Table 4. It can be seen that for a given oxidation state, the carbon−carbon separations are not significantly altered by variation in the metal−ligand composition. We simply note a very small contraction of the C(α)−C(β) contact (ca. 0.01 Å)

in the carbonyl complexes $\mathbf{7}^{n+}$ and $\mathbf{8}^{n+}$ with respect to those bearing phosphine ligands. In all cases there is the by now familiar expansion of the C(α)−C(β) bonds and contraction of the C(β)−C(β') bonds upon oxidation.

The most significant variation in structural parameters in this series of complexes occurs in the Ru−C(α) distances (Table 4). The replacement of the weak π-acceptor phosphine ligands by the strong π-acceptor carbonyl ligands in $\mathbf{7}^{n+}$ and $\mathbf{8}^{n+}$ and consequent reduction in electron density at the metal centers leads to a further decrease in the back-bonding interactions that occur from the stabilized dπ manifolds of the metal atoms into the π* FMOs of the C_4 chain, resulting in the longer metal−carbon separations. However, regardless of the surrounding ligands tethered to the metal atoms, the singlet state electronic configuration is slightly energetically favored over the triplet state electronic configuration in the case of the dicationic species (Table 4), and cumulenic structures may be anticipated for each of $\mathbf{4}^{2+}$, $\mathbf{5}^{2+}$, $\mathbf{6}^{2+}$, $\mathbf{7}^{2+}$, and $\mathbf{8}^{2+}$. Similar energies are computed for model $\mathbf{7}^{2+}$ with HS and LS configurations.

The molecular orbital compositions and energy levels of the neutral model complexes as a function of the metal−ligand fragments are illustrated in Figure 9. Model complexes **4**−**6** exhibit electronic properties remarkably similar to those of complex **3-H**. The energy level schemes associated with these compounds are practically identical, with the HOMOs of a′ and a″ symmetry separated from both the high-lying LUMOs and, to a lesser extent, from the low-lying metal-based occupied MOs. In contrast to the limited changes observed upon substitution of Cp for Cp*, or PH_3 for dHpe, a more significant effect is observed when the phosphine ligands PH_3 or dHpe are replaced by carbonyl ligands. In particular, an important shift to lower energy is computed for MOs in the carbonyl compounds **7** and **8**. Nevertheless, their orbital schemes are qualitatively similar to those for models containing phosphine ligands with HOMOs lying in the middle of an energy gap separating high-lying antibonding MOs from low-lying metal-based nonbonding MOs (Figure 9). HOMO/LUMO gaps are similar in all models (ca. 1.7 eV). As a result of the π-acceptor character of the carbonyl ligand in **7** and **8**, the metal-to-carbon chain π-type back-bonding contribution to the HOMOs in these complexes is reduced. Consequently, a comparison of the metal vs carbon percentage contribution to the HOMOs reveals that the replacement of phosphine ligands by carbonyl groups yields HOMOs more heavily weighted on the carbon bridge. This reflects in Hirshfeld atomic charges which indicate that electron density loss of the carbon atoms upon oxidation is more important in models **7** and **8** than in models bearing phosphine groups (Table 6).

Ionization Potentials. While experimental photoelectron spectra have not yet been reported for the Ru_2C_4-based molecules described in this work, the present calculations on $[\mathbf{3\text{-}H}]^{n+}$ ($n = 0-4$) and the other related model complexes may be used to predict the gas-phase ionization potentials (IP). The adiabatic IPs computed for model complexes $[\mathbf{3\text{-}H}]^{n+}$ and $\mathbf{4}^{n+}$−$\mathbf{8}^{n+}$ are compared in Table 4. They correspond to removal of electrons housed in the HOMOs of a′ and a″ symmetry. The IPs are considerably lower in the case of complexes **3-H** and **4-6**, which contain phosphine ligands, than in the carbonyl complexes **7** and **8**. This indicates that the presence of strong σ-donor ligands as surrounding ligands, i.e., rather electron-rich metal centers, favor low IPs. The lowest IPs are computed for model **6** which contains Cp* and dHpe, both electron-donating groups.

In principle, redox potentials may be related to ionization potentials by adding the differences between the solvation energies of the reduced and oxidized species to the IPs of the reduced species and correcting for the potential of the reference electrode.[19] A plot of IPs computed for **3-H** vs oxidation potentials experimentally measured for **3-Ph** shows a linear correlation (Figure 11). Assuming comparable solvation energies for $[\mathbf{3\text{-}H}]^{n+}$ and $\mathbf{6}^{n+}$, a plot of the IPs computed for **6** on this curve indicates that successive oxidations of complexes containing electron-donating Cp* and diphosphine ligands should be easier with a negative shift of ca. 0.15 V of the redox potentials with respect to those measured for species **3-Ph**. The increasing ease of oxidation with strong electron-donating groups tethered to the metal centers is in accord with the electrochemical results showing that complex **3-Me** is more readily oxidized than complex **3-Ph** (vide supra).

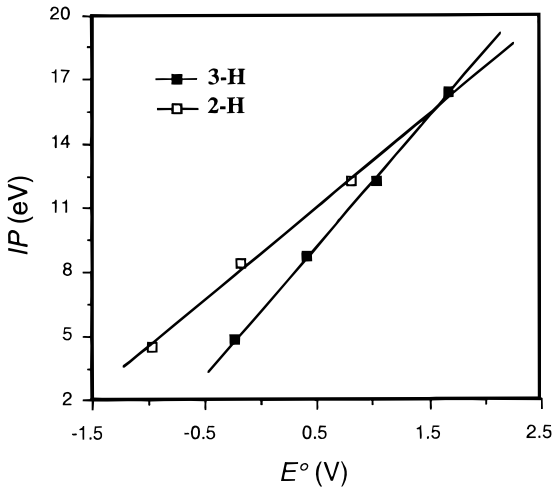

Figure 11. Successive ionization potentials (IP) computed for models $\{Cp(PH_3)_2Ru\}_2(\mu\text{-}C_4)$ (**3-H**) and $\{Cp(PH_3)_2Fe\}_2(\mu\text{-}C_4)$ (**2-H**) vs redox potentials ($E°$) measured for $\{Cp(PPh_3)_2Ru\}_2(\mu\text{-}C_4)$ (**3-Ph**) and $\{Cp*(dippe)Fe\}_2(\mu\text{-}C_4)$, respectively.

IPs are also dependent on the nature of the metal centers. The first and second IPs computed for the iron model **2-H** are lower than the corresponding ones for **3-H**. The third IP is nearly similar in both models, whereas the fourth becomes larger in **2-H** with respect to **3-H**.[39] This is agreement with electrochemical data found for the iron and ruthenium compounds **2** and **3**.[20,23] The first and second oxidation waves occur at potentials slightly less positive for species **2** with respect with species **3**. On the other hand, the third oxidation wave is observed at almost the same potential for both compounds. The fourth oxidation step has not yet been reported for the iron complexes.[23] The plot of IPs computed for $[\mathbf{2\text{-}H}]^{n+}$ vs experimental redox potentials of $[\{Cp*(dippe)Fe\}_2(\mu\text{-}C_4)]^{n+}$ (Figure 11) suggests that the fourth oxidation would occur over 2 V (vs SCE), a value outside the potential windows of most solvents commonly used for electrochemical studies.

Conclusion

We have shown that the neutral complexes **3-Ph** and **3-Me**, which contain a C_4 chain end-capped by $Ru(PR_3)(PPh_3)Cp$ (R = Ph or Me) moieties, can be oxidized to give a series of mono-, di-, tri-, and tetracations. Theoretical calculations indicate that oxidation of compounds **3** affects both the metal centers and the carbon atoms of the C_4 bridge, since this process corresponds to the removal of electrons housed in MOs delocalized over all atoms of the Ru−C_4−Ru chain. Comparison of models with different ligand surroundings suggests that molecules containing

strong electron-donating ligands should be the more readily oxidized.

Experimental Section

General Experimental Conditions. All reactions were carried out under dry, high-purity nitrogen unless otherwise stated, using standard Schlenk techniques. Solvents were dried and distilled according to convention. Elemental analyses were preformed by the Canadian Microanalytical Service, Delta, BC, Canada.

Instrumentation. IR spectra in Nujol were obtained from samples mounted between NaCl disks with a Perkin-Elmer 1720X FT IR spectrometer. NMR spectra were recorded on Bruker ACP 300 (^{1}H at 300.13 MHz, ^{13}C at 75.47 MHz) or Varian Gemini 200 (^{1}H at 199.8 MHz, ^{13}C at 50.29 MHz) spectrometers. Samples were dissolved in $CDCl_3$ (Sigma). Electrospray mass spectra (ES MS) were obtained from samples dissolved in MeOH unless otherwise indicated. Solutions were injected into a VG Platform II spectrometer via a 10 mL injection loop. Nitrogen was used as the drying and nebulizing gas. Samples were examined at cone voltages in the range 20−80 V to find the best conditions. Chemical aids to ionization are indicated where used.[42] The IRRAS and OTTLE cells have been described in detail previously.[27,28] The IRRAS spectra were collected on a Bio-Rad FTS 60A model spectrometer from samples held at −50 °C, and OTTLE spectra from the NIR to UV were collected on a Perkin-Elmer Lambda 9 spectrometer at −30 °C.

Reagents. $\{Cp(PPh_3)_2Ru\}_2(\mu\text{-}C_4)$ (**3-Ph**)[24,26] and PMe_3 [43] were prepared by the literature methods. $AgPF_6$ was purchased (Pennwalt) and used as received. Solvents were dried and distilled prior to use according to convention.

Preparation of $\{Cp(PPh_3)(PMe_3)Ru\}_2(\mu\text{-}C_4)$ (3-Me). A Carius tube was charged with **3-Ph** (150 mg, 0.10 mmol), toluene (5 mL), and PMe_3 (110 μL, 1.2 mmol) and sealed under vacuum. The tube was heated at 120 °C for 4 d to give a translucent orange solution. The tube was opened, and the solvent was removed in vacuo. The oily residue obtained was triturated with hexane under a N_2 stream to give **3-Me** as an somewhat air-sensitive yellow powder (45 mg, 43%). Anal. Found: C, 63.43; H 5.38. Calcd for $C_{56}H_{58}P_4Ru_2$: C, 63.64; H, 5.49. IR (Nujol): ν(C≡C) 1974 cm^{-1}. ^{1}H NMR: δ 7.70−7.15 (15H, m, Ph), 4.43 (5H, s, Cp), 1.17 (9H, br, PMe_3). ^{13}C NMR: δ 134.34−127.32 (m, Ph), 82.71 (s, Cp), 22.50 (br, PMe_3). ES MS (*m*/*z*): 1058, M^+; 796, $[M - PPh_3]^+$; 505, $[Ru(PMe_3)(PPh_3)Cp]^+$.

Preparation of $[\{Cp(PPh_3)_2Ru\}_2(\mu\text{-}C_4)][PF_6]$ ([3-Ph][PF$_6$]). A rapidly stirred solution of **3-Ph** (500 mg, 0.35 mmol) in CH_2Cl_2 (50 mL) was treated dropwise with a solution of $AgPF_6$ (89 mg, 0.35 mmol) in 1,2-dimethoxyethane (10 mL). The resulting deep green solution was filtered through a pad of Celite to remove the precipitated Ag metal, and the solvent was removed from the filtrate. The residue was taken up in a small volume of fresh CH_2Cl_2 and filtered into rapidly stirred Et_2O. The resulting precipitate was collected, washed with Et_2O (3 × 10 mL), and dried to give [**3-Ph**][PF_6] (400 mg, 73%) as a forest-green powder. Anal. Found: C, 65.45; H, 4.36. Calcd for $C_{86}H_{70}F_6P_5Ru_2$: C, 65.52; H, 4.44. IR (Nujol): ν(CC) 1861, ν(PF) 861 cm^{-1}. ^{1}H NMR: δ 7.3−7.1 (br, Ph), 5.0 (br, Cp). ES MS (*m*/*z*): 1430, $[\{Cp(PPh_3)_2Ru\}_2(C_4)]^+$; 691, $[Ru(PPh_3)_2Cp]^+$.

Preparation of $[\{Cp(PPh_3)_2Ru\}_2(\mu\text{-}C_4)][PF_6]_2$ ([3-Ph][PF$_6$]$_2$). Complex **3-Ph** (500 mg, 0.35 mmol) in CH_2Cl_2 (50 mL) was treated with a solution of $AgPF_6$ (221 mg, 0.88 mmol) in 1,2-dimethoxyethane (20 mL) in dropwise fashion. During the addition the color of the solution changed from orange through deep green to dark blue. The solvent was removed and the residue extracted with a small volume of fresh CH_2Cl_2. The extracts were filtered into stirred hexane, and the resulting dark blue precipitate was crystallized (CH_2Cl_2/pentane) to give [**3-Ph**][PF_6]$_2$ as a dark blue microcrystalline solid. Anal. Found: C, 60.57; H, 4.37. Calcd for $C_{86}H_{70}F_{12}P_6Ru_2$: C, 60.07; H, 4.07. IR (Nujol): ν(CC) 1766, ν(PF) 860 cm^{-1}. ^{1}H NMR: δ 7.70−7.07 (m, 30H, PPh_3); 5.03 (s, 5H, Cp). ^{13}C NMR: δ 133.94−128.80 (m, Ph), 90.82 (s, Cp). ES-MS (*m*/*z*): 715, $[\{Cp(PPh_3)_2Ru\}_2(C_4)]^{2+}$.

Mid-IR Spectra (IRRAS Cell). A solution of **1** (**3-Ph,** 7 × 10^{-4} M; **3-Me**, 8 × 10^{-4} M) in CH_2Cl_2 containing 0.1 M $[NBu_4]PF_6$ was introduced into the IRRAS cell[27] and purged with dry N_2. A thin film (ca. 20 μm) of sample solution was trapped between the Pt disk working electrode (3 mm diameter), which was held at −0.22/−0.20 V (**3-Ph**/**3-Me**) with respect to a platinum wire pseudo-reference electrode, and a CaF_2 window through which the sample beam passed. A piece of Pt gauze served as the counter electrode. The film was cooled to −40 to −50 °C prior to the spectroelectrochemical experiment. Oxidation at +0.22/+0.20, +0.72/+0.70, +1.45/+1.30, and +2.20/+1.70 V served to generate the $\mathbf{3}^+$, $\mathbf{3}^{2+}$, $\mathbf{3}^{3+}$, and $\mathbf{3}^{4+}$ species, respectively. Difference spectra were obtained by subtracting the spectrum of the precursor $\mathbf{3}^{(n-1)+}$ complex from that of the $\mathbf{3}^{n+}$ species being investigated. Reversibility was verified by reduction at a potential 0.20 V lower than that used during the oxidation step, and regeneration of the precursor.

Near-IR, Vis, and UV Spectra (OTTLE Cell). Solutions of **3** (**3-Ph**, 7 × 10^{-4} M; **3-Me**, 2.8 × 10^{-3} M) in CH_2Cl_2 containing 0.5M $[NBu_4]BF_4$ were rigorously purged of dissolved oxygen by a passage of a stream of dry N_2 then introduced to the OTTLE cell[28] held at −0.20/0.0 V (**3-Ph**/**3-Me**). A Pt gauze working electrode, Pt wire counter electrode, and a Ag/AgCl reference electrode were employed. The OTTLE cell was mounted in a cryostatic cell block and cooled to −30 °C by means of a stream of cold, dry nitrogen. Electrolysis at +0.20/+0.20, +0.66/+0.60, and +1.32/+1.26 V gave the $\mathbf{3}^+$, $\mathbf{3}^{2+}$, and $\mathbf{3}^{3+}$ species, respectively. Reversiblity was verified by the observation of well-defined isosbestic points and the recovery of clean spectra following electrolytic reduction.

Theoretical Calculations. Extended Hückel calculations were carried out on model $\{Cp(PH_3)_2Ru\}_2(\mu\text{-}C_4)$, **3-H**, of C_{2h} symmetry within the extended Hückel formalism[44] using the program CACAO.[45] Standard atomic distances were taken. The exponents (ζ) and the valence shell ionization potentials (H_{ii} in eV) were respectively the following: 1.3, −13.6 for H 1s; 1.625, −21.4 for C 2s; 1.625, −11.4 for C 2p; 1.6, −18.6 for P 3s; 1.6, −14.0 for P 3p; 2.078, −8.6 for Ru 5s; 2.043, −5.1 for Ru 5p. The H_{ii} value for Ru 4d was at −12.2. A linear combination of two Slater-type orbitals with exponents $\zeta_1 = 5.378$ and $\zeta_2 = 2.303$ with the weighting coefficients $c_1 = 0.5340$ and $c_2 = 0.6365$ was used to represent the Ru 4d atomic orbitals.

Density functional calculations were carried out on models **3-H** and **4-10** using the Amsterdam density functional (ADF) program[46] developed by Baerends and co-workers.[47] The Vosko−Wilk−Nusair parametrization[48] was used for the local density approximation (LDA) with gradient corrections for exchange (Becke88)[49] and correlation (Perdew86).[50] C_s symmetry was chosen for the partially optimized models in order to differenciate the ruthenium centers. The geometry optimization procedure was based on the method developed by Versluis and Ziegler.[51] The atom electronic configurations were described by a double-ζ Slater-type orbital (STO) basis set for H 1s, C 2s and 2p, and P 3s and 3p, augmented with a 3d single-ζ polarization function for the carbon atoms of the organic bridge. A triple-ζ STO basis set was used for Ru 4d and 5s, augmented with a single-ζ 5p polarization function. A frozen-core approximation was used to treat the core electrons of C, O, P, and Ru.[47] Adiabatic ionization potentials were defined as the energy difference between optimized geometries of the reduced and oxidized species.

(42) (a) Nicholson, B. K.; Henderson, W. *J. Chem. Soc., Chem. Commun.* **1995**, 2531. (b) Henderson, W.; McIndoe, J. S.; Nicholson, B. K.; Dyson, P. J. *Chem. Commun.* **1996**, 1183. (c) Henderson, W.; McIndoe, J. S.; Nicholson, B. K.; Dyson, P. J. *J. Chem. Soc., Dalton Trans*. **1998**, 519.

(43) Luetkens, M. F., Jr.; Sattelberger, A. P.; Murray, H. H.; Basil, J. D.; Fackler, J. P. *Inorg. Synth.* **1989**, *26*, 7.

(44) Hoffmann, R. *J. Chem. Phys.* **1963**, *39*, 1397.

(45) Mealli, C.; Proserpio, D. *J. Chem. Educ.* **1990**, *67*, 399.

(46) *Amsterdam Density Functional (ADF) Program*, release 2.3; Vrije Universteit: Amsterdam, The Netherlands, 1997.

(47) (a) Baerends, E. J.; Ellis, D. E.; Ros, P. *Chem. Phys.* **1973**, *2*, 41. (b) Baerends, E. J., Ros. P. *Int. J. Quantum. Chem.* **1978**, *S12*, 169. (c) Boerrigter, P. M.; te Velde, G.; Baerends, E. J. *Int. J. Quantum Chem.* **1988**, *33*, 87. (d) te Velde, G.; Baerends, E. J. *J. Comput. Phys.* **1992**, *99*, 84.

(48) Vosko, S. H.; Wilk, L.; Nusair, M. *Can. J. Phys.* **1980**, *58*, 1200.

(49) Becke, A. D. *Phys. Rev.* **1988**, *A38*, 3098.

(50) Perdew, J. P. *Phys. Rev.* **1986**, *B33*, 8822; **1986**, *B34*, 7406 (erratum).

(51) Verluis, L.; Ziegler, T. *J. Chem. Phys.* **1988**, *88*, 322.

Acknowledgment. Financial support of this work by the Australian Research Council is gratefully acknowedged. P.J.L. held an Australian Postgraduate Award. K.C. and J.-F.H. thank the Centre de Ressources Informatiques (CRI) of Rennes and the Institut de Développement et de Ressources en Informatique Scientifique (IDRIS-CNRS) of Orsay (Project 970649) for computing facilities. We thank Prof. B. K. Nicholson (University of Waikato, Hamilton, New Zealand) for the ES MS data. Thanks are expressed to Prof. J.-Y. Saillard (Rennes, France) and a reviewer for helpful comments.

JA992002T